

FABRICATION OF HIGH DENSITY ALUMINA CERAMICS FROM
NANOPOWDERS THROUGH COLLOIDAL PROCESSING

A THESIS SUBMITTED TO
THE GRADUATE SCHOOL OF NATURAL AND APPLIED SCIENCES
OF
MIDDLE EAST TECHNICAL UNIVERSITY

BY

HÜSEYİN UTKUCAN KAYACI

IN PARTIAL FULFILLMENT OF THE REQUIREMENTS
FOR
THE DEGREE OF MASTER OF SCIENCE
IN
METALLURGICAL AND MATERIALS ENGINEERING

JANUARY 2020

Approval of the thesis:

**FABRICATION OF HIGH DENSITY ALUMINA CERAMICS FROM
NANOPOWDERS THROUGH COLLOIDAL PROCESSING**

submitted by **HÜSEYİN UTKUCAN KAYACI** in partial fulfillment of the requirements for the degree of **Master of Science in Metallurgical and Materials Engineering Department, Middle East Technical University** by,

Prof. Dr. Halil Kalıpçılar
Dean, Graduate School of **Natural and Applied Sciences**

Prof. Dr. C. Hakan Gür
Head of Department, **Met. and Mat. Eng.**

Assist. Prof. Dr. Simge Çınar
Supervisor, **Met. and Mat. Eng., METU**

Examining Committee Members:

Prof. Dr. Caner Durucan
Met. and Mat. Eng., METU

Assist. Prof. Dr. Simge Çınar
Met. and Mat. Eng., METU

Assist. Prof. Dr. Emre Büküşoğlu
Chemical Engineering, METU

Prof. Dr. Bora Maviş
Mechanical Engineering, Hacettepe University

Prof. Dr. Hüsnü Emrah Ünalın
Met. and Mat. Eng., METU

Date: 15.01.2020

I hereby declare that all information in this document has been obtained and presented in accordance with academic rules and ethical conduct. I also declare that, as required by these rules and conduct, I have fully cited and referenced all material and results that are not original to this work.

Name, Surname: Hüseyin Utkucan Kayacı

Signature:

ABSTRACT

FABRICATION OF HIGH DENSITY ALUMINA CERAMICS FROM NANOPOWDERS THROUGH COLLOIDAL PROCESSING

Kayacı, Hüseyin Utkucan
Master of Science, Metallurgical and Materials Engineering
Supervisor: Assist. Prof. Dr. Simge Çınar

January 2020, 82 pages

Utilizing nanopowders in production of fully dense materials with fine grain structures is highly advantageous, particularly where high mechanical properties are desired. Besides, recently developed techniques, such as 3D-printing of ceramics, may require high solids content suspensions. Despite the advantages of slurry based processing of oxide ceramics, production of nano-structured high density bodies is still a challenge. The main limitation in colloidal processing of nanopowders is their unexpectedly high suspension viscosities. High viscosities restrict the maximum achievable solids content, which, in turn, limit the structural integrity and the density of a green body when consolidated. Furthermore, because of the smaller interparticle distance in highly loaded suspensions, nanopowders tend to agglomerate fast, which creates another challenge in terms of the homogeneous distribution of powders in their suspensions and in green bodies. In this thesis, various approaches for nanopowder suspension formulations were discussed and their effect on the particle packing, green body formation and sintering process were investigated. Suspensions with solids content up to 35-40 vol% were obtained. When these suspensions are slip casted, the green body densities as high as 58% could be obtained. When sintered, the structures with relative densities up to 96% could be achieved and that can be further increased

to 99% using α -Al₂O₃ seed powder during sintering. As a result, high density alumina ceramics could successfully be fabricated from nanopowders.

Keywords: Colloidal processing of nanopowders, inter-particle spacing, hydration layer, nanopowder packing, high density alumina

ÖZ

NANOTOZLARDAN KOLLOİDAL YÖNTEMLER İLE YÜKSEK YOĞUNLUKLU SERAMİKLERİN ÜRETİMİ

Kayacı, Hüseyin Utkucan
Yüksek Lisans, Metalurji ve Malzeme Mühendisliği
Tez Danışmanı: Dr. Öğr. Üyesi Simge Çınar

Ocak 2020, 82 sayfa

Nanotozların, yüksek yoğunluklu ve ince taneli malzemelerin üretiminde kullanılması, yüksek mekanik özelliklerin ve/veya 3B Seramik Baskı gibi yüksek katı içerikli uygulamaların gerekli olduğu durumlarda oldukça avantajlıdır. Oksit seramiklerin çamur bazlı üretim süreçleri ile üretimi oldukça avantajlı olmasına karşın, nano-yapılı, yüksek yoğunluklu malzemelerin bu yöntem ile üretimi hala problemlidir. Nanotozların kolloidal süreçler ile üretimindeki en büyük sınırlama, nanotoz süspansiyonlarının beklentilerden de yüksek viskoziteleridir. Yüksek viskozite değerleri, elde edilebilecek en yüksek katı yükleme oranını kısıtlar ki bu da konsolide edilen yaş seramik kütlelerin bütünlüğünü ve yoğunluğunu kısıtlamaktadır. Dahası, yüksek toz yüklemeli süspansiyonlarda parçacıklar arasındaki mesafeler azaldığı için nanotozlar çok daha hızlı topaklanma eğilimi göstermekte ve bu da tozların süspansiyon içerisinde ya da konsolide edilmiş yaş kütlelerde tozların homojen dağılımı ile ilgili zorluklar doğurmaktadır. Bu tez çalışmasında süspansiyon reçeteleri için geliştirilen farklı yaklaşımlar tartışılmış ve bu yaklaşımların parçacıkların dizilimi, yaş kütlelerin oluşumu ve sinterleme sürecindeki etkisi incelenmiştir. Hacimce 35-40%'a varan katı yükleme oranına sahip süspansiyonlar üretilmiştir. Bu süspansiyonların dökümü yapıldığında 58%'e varan ön yoğunluğa

sahip yaş kütleler üretilmiştir. Sinterleme sonucu yoğunluklar 96%'ya kadar yükseltilmiş ve α -Al₂O₃ çekirdekleri süspansiyona eklendiğinde son yoğunluk 99% olarak ölçülmüştür. Sonuç olarak, nanotozlardan yüksek yoğunluklu alümina seramikleri başarıyla üretilebilmiştir.

Anahtar Kelimeler: Nanotozların kolloidal süreçleri, parçacıklararası uzaklık, hidrasyon katmanı, nanotoz paketlemesi, yüksek yoğunluklu alumina

To my family, Őükrü and Selma KAYACI, who do not refrain their full support and
endless love under any circumstances...

ACKNOWLEDGEMENTS

I am deeply thankful to my advisor, Dr. Simge ÇINAR, for her patience, support and supervision which enwidened my vision and research perspective throughout my research. She consistently supported me to do this thesis as my own work and steered me in the right the way whenever I needed it.

I would like to thank my thesis committee: Prof. Dr. Caner DURUCAN, Assist. Prof. Dr. Emre BÜKÜŞOĞLU, Prof. Dr. Bora MAVİŞ and Prof. Dr. Hüsnü Emrah ÜNALAN for their encouragement, insightful and supportive comments.

I would also like to thank Prof. Dr. Müfit AKINÇ and Prof. Dr. Arcan Fehmi DERİCİOĞLU. The door of Professors' office were always open to me whenever I had a question and I needed to use laboratory facilities.

I must express my heartily gratitude to my brother/sister-like friends Mertkan MERT, Tufan GÜMÜŞLÜ, Urfani Savaş BEKDAŞ, Gamze ALTAY, Eser Ece ALTINKAYA, Tolga Han ULUCAN and my cousin Yahya Yener AKGÜL for their support and sincere friendship. They were always unquestioningly there when I needed it.

I warmly thank my labmates in Colloids and Smart Materials Laboratory: Bayram YILDIZ, Oğuz GÖZCÜ for the stimulating discussions, being wonderful friends and for being there to endure me to overcome challenges whenever I went through a new one. I would also thank for all the fun we have had in the last two years.

Last but not the least, I would like to specially thank my family for their endless love and encouragement throughout my each step of life. This would not have been possible without them.

TABLE OF CONTENTS

ABSTRACT	v
ÖZ	vii
ACKNOWLEDGEMENTS	x
TABLE OF CONTENTS	xi
LIST OF TABLES	xiii
LIST OF FIGURES.....	xiv
CHAPTERS	
1. INTRODUCTION	1
2. LITERATURE REVIEW	5
2.1. Fundamental Concepts and Basic Terms	5
2.1.1. Electric Double Layer.....	6
2.1.1.1. DLVO Theory of Double Layer.....	8
2.1.2. Interparticle Spacing	10
2.1.3. Effect of Solids Loading on Viscosity of Suspensions.....	11
2.2. Stabilization Mechanisms of Nanopowder Suspensions.....	12
2.2.1. Electrostatic Stabilization	12
2.2.2. Hydration Layer and Its Effect on the Viscosity of Nanopowder Suspensions.....	14
2.2.3. Effective Reduction of Viscosity of Nanopowder Suspensions Using Combination of Mechanisms	17
2.2.4. Steric and Electrosteric Stabilization: Effect of Low and High Molecular Weight.....	18

2.3. Sintering of the Alumina Ceramics.....	24
3. EXPERIMENTAL DETAILS.....	29
3.1. Materials.....	29
3.2. Experimental Methods	30
3.2.1. Preparation of Suspensions	30
3.2.1.1. Preparation of Suspensions with Fructose and NaCl.....	30
3.2.1.2. Preparation of Suspensions with Ascorbic Acid	31
3.2.2. Slip Casting and Sintering of Alumina Bodies	31
3.3. Characterization of Green and Sintered Bodies	32
3.3.1. Green and Sintered Density Measurements	32
3.3.2. Rheology Measurements	33
3.3.3. Scanning Electron Microscopy	33
4. COMBINED EFFECT OF FRUCTOSE AND SODIUM CHLORIDE ON PARTICLE PACKING AND SINTERING BEHAVIOURS	35
4.1. Particle Packing Behaviour.....	35
4.2. Sintering Behaviour	49
4.3. Effect of Seeding on Sintering Behaviour	52
5. EFFECT OF ASCORBIC ACID ON PARTICLE PACKING AND SINTERING BEHAVIOURS.....	57
5.1. Particle Packing Behaviour.....	57
5.2. Sintering Behaviour	61
5.3. Effect of Seeding on Sintering Behaviour	65
6. CONCLUSIONS	69
REFERENCES	73

LIST OF TABLES

TABLES

Table 2.1. Effect of fructose and NaCl and their combined effect on the viscosity of alumina nanopowder suspensions at a constant shear rate of 100 s^{-1} . (xx Al indicates xx vol.% of alumina and yy F, and indicates yy wt.% of fructose additions.).....	18
Table 4.1. IPS estimations for alumina nano and micron sized powders in aqueous media.	37
Table 4.2. Comparative estimations of IPS and available IPS under the effect of HL and EDL with respect to solids content in the absence of NaCl.	39
Table 4.3. Comparative estimations of IPS and available IPS under the effect of HL and EDL with respect to solids content.....	40
Table 4.4. The power law parameters obtained from the rheological behavior of alumina nanopowder suspensions. As additives 4 wt% fructose and 0.01M NaCl were used.	41
Table 4.5. The inter-particle spacing estimations for alumina nanopowders in aqueous solutions (IPS_{aq}). The effect of NaCl concentration were considered for suspensions with solids loading of 0.40 and with fructose addition of 4 wt%. For these suspensions, IP_{HS} and ΔR_{HL} were estimated as 13.1 nm and 3.2 nm, respectively.	46
Table 4.6. Effect of solids content and NaCl concentration on grain size.	50
Table 4.7. Effect of seed amount on grain size.	55
Table 5.1. The power law parameters obtained from the rheological behavior of alumina nanopowder suspensions. As an additive 1 wt% ascorbic acid was used.	58
Table 5.2. Effect of solids content on average grain sizes	63
Table 5.3. Effect of seed amount on grain size of sintered bodies constantly at 0.20 solids content.....	68

LIST OF FIGURES

FIGURES

Figure 1.1. Slurry based production of alumina ceramics.	2
Figure 2.1. Schematical representation of Electric Double Layer.....	8
Figure 2.2. Net interaction energy curve (DLVO curve) between two converging particles. V_R, V_A and V_T represent potential energies of repulsion, attraction and total, respectively.....	9
Figure 2.3. Effect of NaCl concentration on the viscosity of alumina nanopowder suspensions at different solids contents and a constant shear rate of 10 s^{-1}	14
Figure 2.4. (a) DSC curves for pure water (trace a), micrometer size (trace b), and nano size alumina (trace c) suspension with a solids content of 0.30. (b) Effect of fructose concentration on the reduction of viscosity with respect to solids content. (c) Change in bound water fraction with fructose concentration of 20 vol% alumina nano powder suspensions. (d) Direct visualization of hydration layer	16
Figure 2.5. Schematical representation of stabilization mechanisms	19
Figure 2.6. Schematical representation of experimental steps	23
Figure 2.7. (a) Variation of viscosity of 20 vol.% nano alumina suspensions with different concentrations of ascorbic acid as a function of ascorbic acid concentration (b) Effect of ascorbic acid concentration of 1 wt.% on the viscosity as function of solids content at a constant shear rate of 100 s^{-1}	24
Figure 2.8. Effect of sintering time on relative densities and average grain sizes	25
Figure 2.9. Phase transition diagram of Al_2O_3	27
Figure 2.10. Sintered densities of α -seeded $\gamma\text{-Al}_2\text{O}_3$ and $\delta/\alpha\text{-Al}_2\text{O}_3$ samples with respect to seed amount as a function temperature	27
Figure 3.1. (a) TEM micrograph of alumina nanopowder (b) SEM micrograph of seed $\alpha\text{-Al}_2\text{O}_3$ powder	29
Figure 4.1. Schematical comparison of no additive and combined effect on the initial particle packing produced from aqueous alumina nanopowder suspensions. Addition of fructose and NaCl contracts hydration and electric double layers which increases	

available interparticle spacings. Increased interparticle spacings results in close packing compared to its counterpart with insufficient interparticle spacing.	36
Figure 4.2. Kuwabara’s virtual cell was modified in order to account for the effects of electric double layer and the hydration layer. IPS_{HS} is the inter-particle distance with hard-sphere assumption; IPS_{aq} is the inter-particle distance in aqueous solutions. R_p is the radius of particles, ΔR_{EDL} is the Debye length, and ΔR_{HL} is the hydration layer thickness.....	38
Figure 4.3. (a) Change in viscosity with respect to solids content as a function of shear rate and (b) its effects on initial particle packing density	41
Figure 4.4. Effect of contraction of hydration and electric double layers on particle packing behaviour at (a-c) 0.20, (d-f) 0.30, (g-i) 0.40 solids content and their macro-micro-nano structures are given from left to right respectively.....	44
Figure 4.5. (a) Change in Debye Length (K^{-1}) with NaCl concentration and (b) its effect on Net Interaction Energy between particles as a function of distance	45
Figure 4.6. (a) Change in the viscosity with increasing NaCl concentration as a function of shear rate and (b) its effect on the initial particle packing density	47
Figure 4.7. Evolution of microstructure and packing behaviour at 0.40 solids content with increasing NaCl concentrations of (a-c) 0.01 M, (d-f) 0.02 M, (g-i) 0.04 M and their macro-micro-nano structures are given from left to right respectively.	47
Figure 4.8. Effect of solids content and NaCl concentration on the sintered densities	50
Figure 4.9. Effect of solids content and NaCl concentration on the microstructural evolution of sintered Al_2O_3 bodies. Sintered bodies are given as (a) 0.20 – 0.01 M NaCl, (b) 0.30 – 0.01 M NaCl, (c) 0.40 – 0.01 M NaCl, (d) 0.40 – 0.02 M NaCl (e) 0.40 – 0.04 M NaCl, (f) Average grain sizes as a function of solids content.	51
Figure 4.10. Effect of seeding and its amount on the sintered density at 0.20 solids content.....	53
Figure 4.11. Effect of seeding and its amount on the microstructure of sintered bodies at 0.20 solids content. Seed amounts are (a) 3 wt.% (b) 5 wt.% of alumina powder.	54

Figure 5.1. Effect of 1 wt.% ascorbic acid addition on the viscosity of nano-alumina suspensions with various solids content.	57
Figure 5.2. Particle packing densities with respect to solids content at 1 wt.% ascorbic acid concentration.	59
Figure 5.3. (a-c) Macro, (d-f) micro, (g-i) nano structures of bodies having 0.20, 0.30, 0.40 solids content from top to bottom respectively.....	60
Figure 5.4. Effect of solids content on the sintered densities at 1 wt.% ascorbic acid concentration.....	63
<i>Figure 5.5.</i> Microstructures of sintered bodies having (a) 0.20, (b) 0.30, (c) 0.40 solids content respectively	64
Figure 5.6. Effect of seeding and its amount on sintered densities.	66
Figure 5.7. Effect of seeding and its amount on the microstructure of seeding samples having solids content of 0.20. (a) 0 wt.%, (b) 3 wt.%, (c) 5 wt.% of seed powders..	67

CHAPTER 1

INTRODUCTION

Achieving a high density structures are critical for many advanced ceramic applications. For ceramic materials with high mechanical strength, for example, fully dense bodies are required to prevent crack propagation through pores. Besides, near net shape ceramic production techniques such as direct ink writing or robocasting, the use of suspensions with high solid loading and achieving high density products after sintering is critical. [1]

In ceramic processing, starting with finer and spherical particles (curvature effect) is of great significance since it provides higher specific surface area which is the main driving force for diffusion between particles during sintering process. [1] Therefore, the use of nano-sized particles provides great densification rates even at lower sintering temperatures. Therefore, relatively low temperatures with shorter times for sintering processes can be provided and energy costs for processing can be reduced when nanopowders are used. Use of nanoparticles may provide fine-grained final products and enables the production of high strength final products. Moreover, nanoparticles may provide great advantages on the production of thin films or complex shaped products with fine details by increasing controllability of geometric details, which, in turn, enables the applicability of additive manufacturing techniques and thin film studies on ceramics. However, nanoparticles tend to agglomerate in this size range and these agglomeration increases viscosities of nanopowder suspensions and it limits maximum achievable solids content. As a result, homogeneous packing of particles become impossible. This phenomenon results in green body with porous structure and low packing density. [1,2] This level of porosity cannot be removed with sintering process and residual porosity is observed in the final product. Pores remained in the final product act as stress concentrators and diminish its mechanical properties.

In order to reach fully dense structure, successful sintering process must be achieved. To achieve a successful sintering process, process should be controlled from properties of starting powder and preparation of green bodies till the end of sintering process. Typical process of slurry based processing of alumina ceramics can be seen on Fig.1.1.

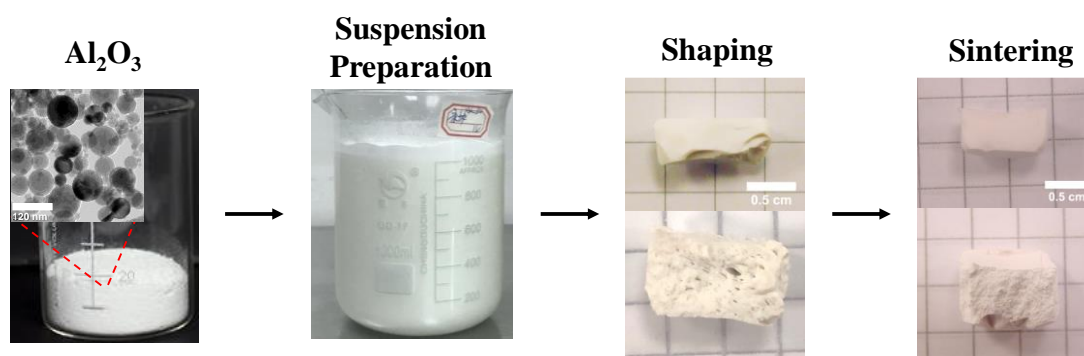


Figure 1.1. Slurry based production of alumina ceramics.

Colloidal processing of ceramics is basically the consolidation of powders from suspensions. For a successful process, the powders should be homogeneously dispersed in a solvent. Dispersants reduce the viscosity of suspensions, thus, allows the increase in solids loading. Since the lower viscosities of suspensions indicate better stabilized powder, suspension formulation is critical in colloidal processing of ceramics. Suspensions with homogeneously dispersed powders and optimum solids content leads to high packing efficiency in green bodies after solvent evaporation. This high efficiently packed green bodies, then, can be sintered to poreless bodies.

Even though suspension preparation of nanopowder suspensions and sintering processes have been widely studied in literature, there are not many examples where fabrication of fully dense structures from nanopowders was reported. Besides, the effect of suspension properties on packing behavior and green body formation is overlooked. Therefore, the main aim of this study to fill the gap between the studies

on suspension preparation and sintering in order to formulate a procedure to obtain high density ceramics from nanopowders.

To this end, the stabilization mechanism of alumina nanopowder suspensions reported in literature is reviewed (Chapter 2). Then the two most effective stabilization mechanisms (combined effect of fructose and NaCl, ascorbic acid additions) were studied in detail in terms of their effect on particle packing behaviour, green body formation and sintered products.

The experimental details of the study is presented in Chapter 3. The case of combined addition of fructose and NaCl is discussed in Chapter 4 and the case of ascorbic acid is presented in Chapter 5, these two mechanisms are also compared.

CHAPTER 2

LITERATURE REVIEW

2.1. Fundamental Concepts and Basic Terms

Suspension term refers to liquid containing suspended solid particles and *colloid* is distinctly dispersed phase from one another and this term used for phase moving with Brownian motion. In solid-liquid colloids, the particle size is commonly in the range from 1 to 1000 nm in aqueous suspensions of oxide particles in order to overcome gravitational effects. [1]

Since gravitational forces are more dominant on micron sized particles, controlling its rheological behaviour is a challenge. Therefore, homogeneous particle packing in consolidation can not be easily achieved. This problem revealed the importance of finer sized particles in sub-micron and nano size range which can suspend in suspensions in the production of fully dense structured ceramics. Besides, when sub-micron sized and nano sized particles are compared, the fact that nano sized particles are more advantageous in sintering stands out due to the Herring's Scaling Law: [3,4]

$$\frac{\Delta t_1}{\Delta t_2} = \left(\frac{R_1}{R_2}\right)^m \quad (2.1)$$

where 1 and 2 represents two different powders, t is sintering time, R is radius and m (1 to 4 depending on transport mechanism) is transport mechanism. From this relation, it can be seen that required sintering time is shortened with finer particles. It was also known that nano particles can be sintered at lower sintering temperatures due to its higher diffusivity arising from its extremely high specific surface area which enables higher number of point of contacts. [1] Moreover, nanoparticles can produce finer grain sized microstructures compared to their sub-micron counterparts.

Achieving high solids content in suspensions takes very important place in the production of advanced ceramics to eliminate shape distortions occurring in complex detailed products and cracks which can occur during green body consolidation because dilute suspensions show severe drying due to the higher solvent content. Moreover, production of complex shaped ceramics and use of techniques that can produce these complex shapes like additive manufacturing can only be possible with high solids content. However, controlling the colloidal processing becomes more important and more complex with finer particles and at higher solids loading. To clarify this complexity and their effects on particle packing, the behaviour of nanopowders in solutions is discussed based on the electric double layer formation, DLVO theory, interparticle spacings, stabilization mechanisms and their effects on flow and the effect of suspension preparation.

2.1.1. Electric Double Layer

Alumina ceramics are sparingly soluble in water. This slight solubility generates unequal distribution of anions and cations around the particles and powders are charged with positive charges. Exact opposite of this positive charge is developed on the surface of particles. [5] As a result, a layer is formed around particles. This inner layer which is close to the surface with opposite charge of particles is called *Stern layer*. Second layer which is extending through the bulk of the solution is called *slipping plane*. With increasing distance from the surface, charge density gradually decays through zero. [1]

The term *Electric Double Layer* (EDL) is used to describe this phenomena. Fig.2.1 shows schematical representation of EDL. In this figure, ions belong to the particle, which are chemisorbed units, are called *potential determining* or *charge determining ions*, while other ions, which does not specifically adsorb on the surface but attracted or repelled by the surface, are called *indifferent ions*. [1] In the presence of potential determining ions in homogeneous suspensions, there will be no net charge on the surface when pH of the solution is at the *isoelectric point* of the oxide. Isoelectric point

of Al_2O_3 was reported as pH of 8-9. [6] When pH is different from isoelectric point, a net charge on the oxide particle will be in positive or negative depending on the suspension pH with respect to the isoelectric point of powder. This net potential charge is measured on the slipping plane and it is called *zeta potential* which is a term used to interpret repulsive ability of particles.

On the quantitative analysis of experimental stabilization of suspensions, Rand and Fries [7] revealed a highly important effect of the thickness of *electric double layer* on nanopowder suspensions. They reported that when the ionic strength of the suspensions was low, viscosity was a couple of orders of magnitude higher than the viscosity of suspensions with high ionic strength. It was attributed to contraction in *double-layer thickness*. They showed that effective solids content was reduced with decreasing double layer thickness which provided more available space for easier flow of particles. In fact, it was a well-known phenomenon for micron and sub-micron suspensions that the viscosity increased with increasing ionic strength, however, the study reported by Rand and Fries [7] claims the exactly opposite behaviour for nanopowder suspensions. On this context, Schneider *et al.* [8] reported that impact of interparticular interactions on the viscosity becomes much more important as particles got finer in size, because these interacting double layers become much more effective on the rheology of nanopowder suspensions. Thus, it can be concluded that the effect of electric double layer on alumina ceramics has to be better understood in a more comprehensive manner.

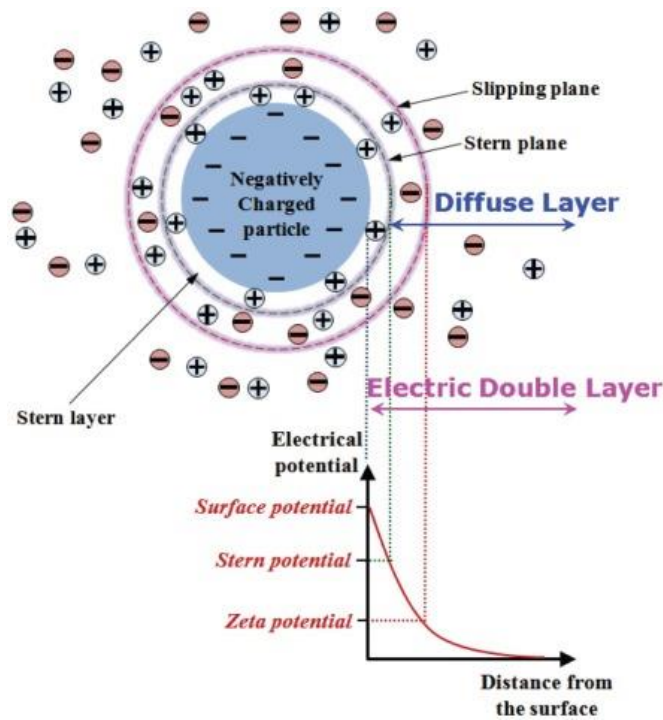


Figure 2.1. Schematic representation of Electric Double Layer. Retrieved from [9]

The theory which predicts the stability of powders based on the balance between the effective attractive and repulsive forces is called *DLVO Theory*. [10,11]

2.1.1.1. DLVO Theory of Double Layer

The scientists Derjaguin and Landau from Soviet Union [12], and Verwey and Overbeek from Netherlands [13], developed at the same time but independently this theory which explains colloidal stability by using attractive and repulsive forces acting on the surface of particles. [11] This theory is very similar to the interaction between two bonded atoms with a scale difference. In this case, electric double layers overlap and repulse each other. Here, repulsive energy between two particles at $2d$ distance is given by: [1,10,14]

$$\Phi_R = \frac{64\eta_0 kT \gamma_0^2}{K} \exp(-K2d) \quad (2.2)$$

where η_0 is the concentration of ions in the bulk, k is the Boltzmann constant, T is the

temperature in Kelvin, γ_0 is the surface charge. Here, K term refers to the reverse of the thickness of electric double layer and called *Debye length*. Debye length is determined from: [1,10,14]

$$K^{-1} = \left(\frac{N_A e^2 I}{\epsilon \epsilon_0 k T} \right)^{-\frac{1}{2}} \quad (2.3)$$

where N_A is Avogadro's number, e is the electronic charge, I is the ionic strength, ϵ is the dielectric constant of medium, ϵ_0 is the permittivity of the vacuum.

The attraction energy between two spherical bodies is given by: [10,14,15]

$$\Phi_A = \frac{A}{2\pi} (2d^{-2}), \quad (2.4)$$

where A indicates the Hamaker constant of the material. From sum of the two terms, net interaction energy between two particles can be calculated: [10,14,15]

$$\Phi_{\text{Net}} = \Phi_R + \Phi_A = \frac{64\eta_0 k T \gamma_0^2}{K} \exp(-K2d) - \frac{A}{2\pi} (2d^{-2}) \quad (2.5)$$

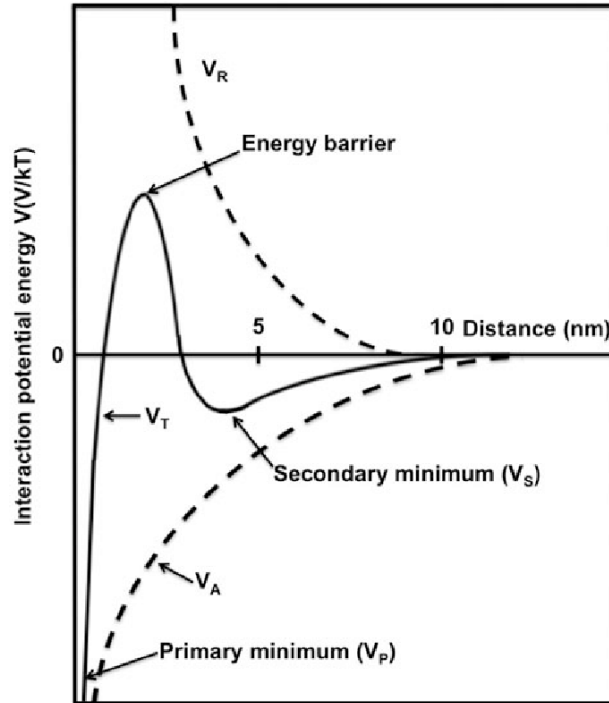


Figure 2.2. Net interaction energy curve (DLVO curve) between two converging particles. V_R , V_A and V_T represent potential energies of repulsion, attraction and total, respectively. Retrieved from [16]

Fig.2.2 [16] shows DLVO curve drawn from the net interaction energy of a materials where V_R , V_A and V_T refers to potential energies of repulsion, attraction and total (net) respectively. On the curve of V_T , it can be concluded that having high energy barrier means better stabilization. When particle interactions cannot overcome the energy barrier, particles are placed on a stable distance called *secondary minimum*. The distance between two particles at maximum total potential energy is the closest point where repulsion is maximum. When interparticle spacing is less than this critical distance, particles agglomerate and cannot be dispersed. As particles agglomerated, their size increases and starts to sediment when gravitational forces cannot be overcome. Such a behaviour leads to heterogeneity in properties of suspensions and the green bodies formed after consolidation.

2.1.2. Interparticle Spacing

Interparticle spacing (IPS) is defined as the distance between the surface of two closest particles in suspension. Funk and Dinger proposed a formula to calculate IPS of the monodispersed hard spheres in suspension: [17]

$$IPS = \frac{D}{3} \times \left(\frac{1}{\Phi} - \frac{1}{\Phi_m} \right) \quad (2.6)$$

where D is the diameter of particles and Φ is the particle volume fraction (solids content) and Φ_m is the 0.64 for random packing of monosized hard sphere particles. As inferred from Eq. (2.6), interparticle spacing decreases linearly decreasing particle size, therefore in suspensions of finer particles, the available space for free flow of particles will be lower compared to larger size particles for same solids content. This spacing will further be reduced when solids content is increased. In consistency with significant obstruction on the ability of free flow, viscosity of suspensions will increase. [17,18] With similar consideration, based on this relation suspension viscosity increases with increasing solids content due to restrained movement of particles.

2.1.3. Effect of Solids Loading on Viscosity of Suspensions

For quantitative comparison of viscosity at different solids loadings, Albert Einstein proposed an empirical *Einstein model* (Eq. 2.7): [19,20]

$$\eta_r = \eta_0(1+2.5\Phi) \quad (2.7)$$

where, η_r and η_0 are the viscosities of suspension and solvent, respectively. Φ represents the volume fraction of solids (solids content). According to Einstein's relation, viscosity increases with increasing solids contents. Although this model clearly shows the effects of solids loading, it was only valid for extremely dilute suspensions of monodisperse and perfectly spherical powders.

Vand [21] proposed *Vand's model* to calculate viscosities for relatively more concentrated suspensions (Eq. 2.8):

$$\eta_r = 1 + 2.5\Phi + K_1\Phi^3 \quad (2.8)$$

where, K_1 is an empirical constant between 2.5 and 9. These empirical models (Eq.(2.7) and Eq.(2.8)) are based on Newtonian behaviour and do not consider interactions between particles which are not good estimations for concentrated and/or nano powder containing suspensions.

Kruger-Dougherty model, which is still one of the most commonly used model, was proposed for closer estimation of the viscosity of concentrated suspensions (Eq. 2.9): [22]

$$\eta_r = \left(1 - \frac{\Phi}{\Phi_m}\right)^{-[\eta]\Phi_m} \quad (2.9)$$

where η_r is the viscosity of the suspension, Φ is the particle volume fraction (solids content) and Φ_m is the 0.64 for random packing of monosized hard sphere particles, $[\eta]$ is intrinsic viscosity which is equal to 2.5 for perfect spheres.

Other researches [23–27] have suggested new models for prediction of suspension viscosities. However, they are either suitable for low solids content suspensions or

underestimate the viscosity of nanopowders and this is still a topic which is being discussed. [28–32]

2.2. Stabilization Mechanisms of Nanopowder Suspensions

In order to obtain low viscosity suspensions with homogeneously dispersed powders and to obtain suspensions with high solids content, stabilization mechanisms gain significant importance. In literature, four different approaches were suggested for effective dispersion of nanopowder suspensions.

- I. Electrostatic Stabilization
- II. Controlling Hydration Layer
- III. Steric Stabilization
- IV. Electrosteric Stabilization

2.2.1. Electrostatic Stabilization

Electrostatic stabilization is basically counterbalancing the attractive van der Waals forces with repulsive Coulomb forces. Forbes *et al.* [33] reported that having a suspension with zeta potential values around ± 30 -40 mV would build energy barriers for stable suspensions. By using this stabilization mechanism, green densities around 60-62% were achieved with slip casting using HNO₃ (25-30 vol.% at pH 4.5) and HCl (22 vol.% at pH 4.5) in alumina nanoparticles. [34,35] Even higher green densities reaching 70% could be typically achieved even in more concentrated suspensions of micron and sub-micron systems. [36,37] However, stable suspensions with solids loading over 25 vol.% could not be achieved with electrostatic stabilization for nanopowder suspensions. [38–41] In this context, Lu [42] reported that net interaction between alumina particles which had a diameter of 55 nm and a zeta potential of 43 mV ended up in flocculation. Even though ± 30 -40 mV was considered enough to stabilize the suspension, flocculation was attributed to the insufficient zeta potential. It was revealed that the required zeta potential for stabilized nanopowder suspensions should be much higher.

More specifically, Iijima and Kamiya [43] reported DLVO calculations and claimed that zeta potential of 177 mV was required to establish a kinetically stable suspension having an average particle size of 30 nm. These calculations showed that required zeta potential values was unreasonably high to establish a stable suspension in these circumstances and showed that electrostatic stabilization was not sufficient on the establishment of stable nanopowder suspensions. Besides, Jailaini *et al.* [5] reported that decrease in particle size ended up in further decrease in zeta potential and suggested the use of steric repulsion mechanism. However, the study of Çınar and Akinc [44] revealed an unexpected level of stability for concentrated suspensions at low ionic strength in alumina nanopowder suspensions by using NaCl. Fig.2.3 shows differences in viscosities of alumina nanopowder suspensions at different solids contents and NaCl concentrations at a constant shear rate of 10 s^{-1} . In this study, it was reported that the contraction of electric double layers, with addition of small electrolyte concentration (NaCl) was responsible in this reduction of viscosity. Although the viscosity could be reduced with NaCl additions, increasing trend in viscosity after optimum concentration because the repulsive ability was reduced with contraction of EDL even though additional interparticle spacing could be provided. As a result, particles could not be dispersed at ion concentrations higher than the optimum value and increasing trend in viscosity appeared. However, no remarkable change in viscosity at 15 vol.% solids content should be noted. This result was attributed to the availability of interparticle spacing.

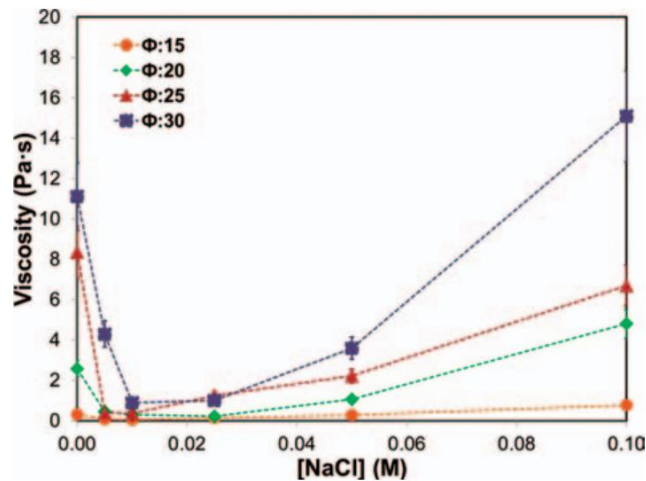


Figure 2.3. Effect of NaCl concentration on the viscosity of alumina nanopowder suspensions at different solids contents and a constant shear rate of 10 s^{-1} . Retrieved from [44]

2.2.2. Hydration Layer and Its Effect on the Viscosity of Nanopowder Suspensions

Hydration layer concept, with the definition used in this thesis, was known as a bound water for a long time without an exact definition. [45–47] The bound water concept was first introduced by Li and Akinc. [48] As shown in Figure 2.4 (a), while pure water shows single melting event as expected, when submicron size alumina powders are added, a little shoulder on the left hand side of the water melting peak is appeared. [49] When nanopowder alumina particles are used, a little shoulder evolved into a distinct second melting event. This secondary phase of water was called *bound water*, and the unexpectedly high viscosities of oxide nanopowder suspensions could be explained with presence of significant amount of bound water. [49] Since the bound water content cannot serve as a solvent, but behaves as a part of the powder, the effective solids content of suspensions becomes much larger than the one used for sample preparation. [49,50]

Katsiris and Kouzeli-Katsiri [51] have shown that any treatment, which could reduce the bound water content in suspension, could effectively reduce the viscosity of nanopowder suspensions. Then, the bound water and its effect on the nanopowder suspension behavior became the point of interest for scientists. Schilling *et al.* [52]

studied the effect of saccharide additions on the viscosity of alumina nanopowder suspensions. They used monosaccharides and disaccharides such as D- fructose, sucrose, and D- glucose and reported that fructose and sucrose additions were very effective in the viscosity reduction while D- glucose was not. Later, Falkowski *et al.* revealed that the effect of saccharides is related with the molecular structure of such molecules and its orientation on oxide surfaces. [53] In further studies, Li and Akinc [48,50] reported that the suspension viscosity remained almost same or slightly changed with and without addition of fructose (18 wt.% by weight of alumina) at solids loading lower than 25 vol.% (Fig. 2.4 (b)). This observation was attributed to the low amount of bound water at low solids loading. When the volume fraction of 28 vol.% without fructose is reached, the viscosity of the suspension started to increase significantly, whereas much sharper increase was obtained at solids content higher than 35 vol.%. After addition of fructose, deceleration in this increasing trend in viscosity was obtained. The effect of bound water content and the fructose addition also given in Fig.2.4 (c).

Recently, Firlar *et. al.* reported the direct visualization of bound water around alumina nanoparticles using the fluid cell STEM in situ. In this study, shown in Fig.2.4 (d), it is revealed that the bound water forms a layer associated with oxide surfaces, therefore the ‘bound water’ term is replaced with the hydration layer [54]. Further studies revealed that hydration layer is formed in various oxide powder suspensions [55] and hydration layer is distinct from the electric double layer [49,56]

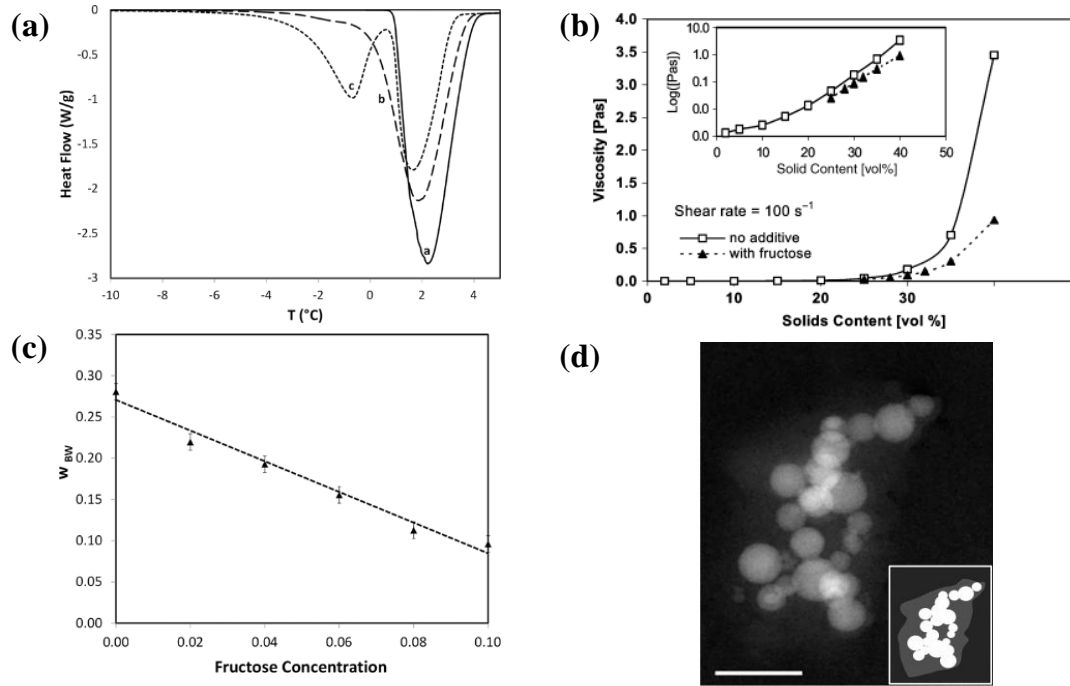


Figure 2.4. (a) DSC curves for pure water (trace a), micrometer size (trace b), and nano size alumina (trace c) suspension with a solids content of 0.30. (b) Effect of fructose concentration on the reduction of viscosity with respect to solids content. (c) Change in bound water fraction with fructose concentration of 20 vol% alumina nano powder suspensions. (d) Direct visualization of hydration layer Retrieved from [49,50,54]

From the data of weight fractions of bound water reported [49,50] by few studies, thicknesses of bound water and contraction in these layers after fructose addition can be calculated by combination of Eq.(2.10) and Eq.(2.11). [49]

$$\Phi_{\text{effective}} = \frac{V_S + V_{BW}}{V_{\text{Total}}} \quad (2.10)$$

where $\Phi_{\text{effective}}$ is effective solids content, V_S , V_{HL} , V_{Total} are volume fractions of solid, hydration layer and total respectively. Since the reported data was weight fraction of bound water, it was assumed that the weight fraction of bound water was equal to the volume fraction due to the density of water (1 g/cm^3). When effective solids content for different solids contents are calculated and it is applied to the Eq.(2.11), thickness of hydration layer are found from:

$$\Phi_{\text{effective}} = \Phi \left(1 + \frac{l}{r}\right)^3 \quad (2.11)$$

where l is thickness of the hydration layer and r is the radius of the particles.

Apart from these studies, Falkowski *et al.* [53] studied the efficiency of reduction of viscosity by addition of monosaccharides on initial particle packing. They reported that green densities around 63-69% could be achieved with addition of fructose from 1 to 5 wt.% of alumina powder to the suspension of 30 vol.%. However, it should be noted that these results were unexpectedly high and effect of rigorousness of experimental steps of the study on particle packing cannot be underestimated. It includes highly meticulous experimental steps during preparation of suspensions. For instance, planetary ball milling was used twice in experimental steps in the mixing of suspensions which would provide efficient particle packing. Between two steps of planetary ball milling, ultrasonication was also used in the preparation steps. Although these additional steps are also successful in the further improvement of particle packing density, it complicates the experimental process, which, in turn, limits its applicability industrial scale.

2.2.3. Effective Reduction of Viscosity of Nanopowder Suspensions Using Combination of Mechanisms

It could be understood that NaCl and fructose were effective on the reduction of viscosity but their effects were limited alone and does not require complicated experimental procedure. Çınar and Akinc [56] reported the combined effect of NaCl and fructose on the reduction of viscosity of alumina nanopowder suspensions. Therefore, both of hydration and electric double layers are modified at the same time. In this study, 4 wt.% of fructose addition was reported as an optimum concentration. Table 2.1 summarizes the effect of fructose, NaCl and their combined effect on viscosity of alumina suspensions with solids loading of 0.20. It clearly reveals that the combined effect of fructose and NaCl facilitates the further reduction of viscosity than sole additions of NaCl or fructose. As presented in Table 2.1, the effect of fructose addition could only decrease the suspension viscosity by 17%. The sole addition of optimum amount of NaCl could decrease. The suspension viscosity by 94% reduction

in viscosity, which could be achieved by contraction of both hydration and electric double layers.

Table 2.1. *Effect of fructose and NaCl and their combined effect on the viscosity of alumina nanopowder suspensions at a constant shear rate of 100 s⁻¹. (xx Al indicates xx vol.% of alumina and yy F, and indicates yy wt.% of fructose additions.) Retrieved from [56]*

Solids content	Viscosity (Pa.s)	Viscosity Reduction (%)
20 Al 00F	0.3922	0
20 Al 04F	0.3254	17
20 Al 00F 0.01 M NaCl	0.0250	94
20 Al 04F 0.01 M NaCl	0.0129	97

The effect of combined addition was studied for solids content of 20 vol.%, however increase in the effectiveness of fructose with increasing solids content can be expected due to the increase in total amount of bound water.

2.2.4. Steric and Electrosteric Stabilization: Effect of Low and High Molecular Weight

Steric stabilization is basically the use of organic molecules to disperse particles. [1,2,14,57] These organic molecules are dissolved in the suspension and/or adsorbed onto the surface of the particles. Effectivity of these chains are attributed to their thermodynamical preferences that these molecules stay in interaction with water molecules, rather than interact with other surfaces. In this context, thickness of the adsorbed layer and the layer coverage are important. When mono-layer coverage of the surface is completed or too long chain molecules are used or IPS is insufficient for dispersion, polymeric additives may cause bridging between particles or depletion which leads to increase in viscosity rather than a decrease.

Electrosteric mechanism can be thought as a combination of the steric and the electrostatic stabilization mechanisms. [1,2,14,57] Fig.2.5 shows the schematical summary of all stabilization mechanisms explained so far. To provide both of the

steric and electrosteric stabilization mechanisms, low and high molecular weight organic additives have widely been studied. [58–63]

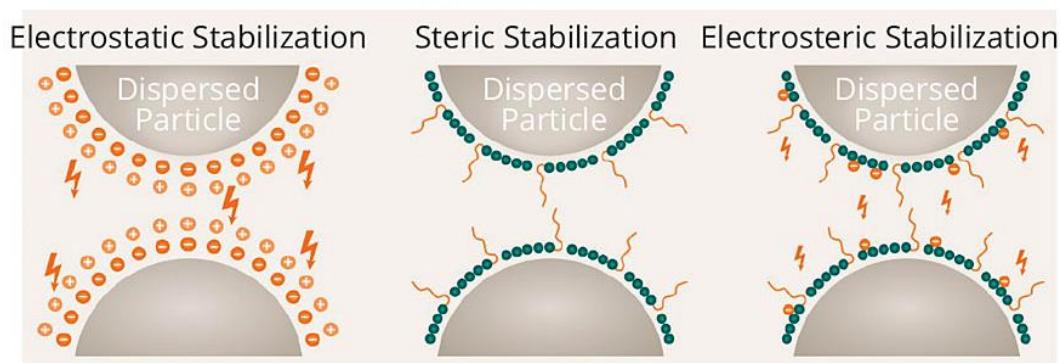


Figure 2.5. Schematical representation of stabilization mechanisms. Retrieved from [64].

Bhosale and Berg [58] reported that the alumina powders having sub-micron sizes could be dispersed effectively using poly(acrylic acid) (PAA (Molecular weight: 2000-10000 g/mol)). Bowen *et al.* [59] also reported similar the effect of PAA (Molecular weight: 2000 g/mol) on viscosity for sub-micron alumina powders. They also showed the initial particle packing efficiency of the Al_2O_3 suspensions dispersed with PAA. It was shown that green density was 36.3% for sub-micron suspensions in the absence of PAA. When the PAA was incorporated into the system, green density could be increased up to 48.9%. Lyckfeldt *et al.* [60] compared the effectivity of PAA (Molecular weight: 4500 g/mol) and a comb copolymer which was poly(oxyethylene) (PEO) in different solvents on the dispersion alumina suspensions. They claimed that concentrated sub-micron Al_2O_3 suspensions with low viscosity could only be achieved in aqueous solvent and suspensions with low viscosities in ethanol or isopropanol could be achieved only up to 25 vol.%. Besides, it was reported that the comb copolymer showed superiority in stabilization compared to PAA. However, no further study has been conducted to reveal its effects on the initial particle packing behaviour. Cesarano and Aksay [65] reported PMAA and PAA (Molecular weights: 1800, 5000, 50000 g/mol) in sub-micron suspensions and reported that highly concentrated suspensions (>50 vol.%) could be stabilized with addition of these dispersants and these polyelectrolytes could stabilize the suspension even in the absence of

electrostatic repulsive forces. It was also reported that green densities over 60% could be achieved with slip casting.

Briscoe *et al.* [66] reported the use of three commercial dispersants ‘Darvan C’, ‘Aluminon’ and ‘Tiron’ in sub-micron suspensions with alumina powders and showed that all of them were capable of producing dispersed system. Darvan C was reported to be the best dispersant among others. No further studies done for their effect on nanopowders or initial particle packing. In other studies, well dispersion and ability of good adsorption of Darvan C onto the surface of alumina were shown. [67,68] Besides, it was shown that initial particle packing density from 30 to 60% could be achieved using Darvan C, depending on the processing, conditions. [69–72] Adsorbability of Tiron and Dolapix on alumina surface were also reported in other studies and shown that high green densities reaching over 60% could be achieved with these dispersants.[36,66,73–75]

Oligo- and polysaccharides have also been studied and suggested for the stability of alumina powders. [37,76–78] Kim *et al.* [37] investigated different commercially available polysaccharides which are different types of maltodextrins and dextrans. They reported that using these stabilizers initial particle packing density of 53.3% and 65.7% was achieved for 20 and 40 vol.% solids content respectively. Additionally, Schilling *et al.* [76] reported that they could achieve green densities of 57% with the help of pressure casting of the suspension which was prepared with maltodextrin.

Apart from these studies, adsorbability and dispersion ability studies of novel dispersants on Al₂O₃ suspensions have also been reported. [79–81] For instance, Cerrutti *et al.* [79] identified lignin as a novel dispersant. They showed that lignin showed effective electrosteric effect at pH of 7 and shifted the isoelectric point of the alumina suspensions to pH of 4.5. In acidic media, lignin did not perform well. In alkaline media, slight stabilizing effect was observed because the electrosteric effect was minimized. In another study, polyaspartic acid (PASP) and polyepoxysuccinic acid (PESA) was reported as novel dispersants. [81] It was shown that both of the

dispersants showed superiority in the dispersion of the suspension. Unfortunately, further studies on the formation of green bodies with addition of these novel dispersants have not been reported and their influence on particle packing behaviour is missing in literature.

To summarize, relative densities of 50-70% in green bodies could be achieved. However, these studies mainly focused on sub-micron systems. Similar densities with same dispersants for oxide nanopowder suspensions could not be reported since the long polymer chains of these additives caused bridging and depletion in highly loaded nanopowder suspensions. [82] Unfortunately, consolidation of cast bodies became problem because of their low density, which, in turn, caused cracks and required more time to dry off. Furthermore, these problems end up in impossibility of widening the range of application areas of nano-alumina suspensions. [2] As an example, the robocasting (3D-Printing of ceramics) requires high yield stress and it can only be provided with high solids loadings. [14,57,82–89] Since high solids loadings cannot be provided, the use of nanopowders and utilizing their highly desirable advantages become impossible. In this context, Kakui *et al.* [90] have revealed that molecular weight of the dispersant had to be less than 1800 for a suspension with particles having average size of 7 nm to achieve same measured viscosity when the dispersant with a molecular weight of 10000 was used in a suspension having sub-micron particle size. These results have clearly showed that the small molecules had to be used in the dispersion of oxide suspensions for steric stabilization of nanopowder suspensions.

Stuart *et al.*[91,92] reported that the dispersant with a chain length of 3-4 nm was required to disperse a suspension having particles of 65 nm. Although small molecules as dispersants have not been studied as widely as high molecular weight dispersants, the use of dispersants such as low molecular weight saccharides, polyalcohols, sugar alcohols, aliphatic and aromatic molecules and their derivatives can be found in the literature.[52,78,93–98] Although some reduction in viscosity were achieved in these studies, reported viscosities were still relatively high to obtain suspensions with high solids contents. In some studies, it was only reported the adsorbability of the molecules

on alumina surfaces but no further studies on their dispersive ability has been reported. In one of the few studies reporting the initial particle packing density, various aliphatic and aromatic dispersants were studied and they reported the slip cast density as high as 50-53%. [78]

Yar *et al.* [99] investigated the use of several polyalcohols as a dispersant for alumina nanopowder suspensions and reported that viscosity of the suspensions with 35 vol.% solids content could dramatically be decreased down by 88% (almost 1 Pa.s at a constant shear rate of 100 s^{-1}) with addition of 10 wt.% polyalcohol but reliability of the reduction in viscosity for higher solids content was not reported. Studart *et al.* [100] studied on the tailor-made Gallol-PEG molecules. They reported that this tailor-made dispersant with head-tail architecture successfully dispersed nanoparticles with average size of 65 nm. They could achieve one of the lowest viscosity values at 30 vol.% solids content in aqueous suspensions (0.13-0.18 Pa.s at a constant shear rate of 100 s^{-1}) and they could obtain stabilized suspensions even at more than 40 vol.% solids contents. However, this dispersant was tailor made since it is not a commercial product meaning that its accessibility and availability in the same quality and property is difficult and its applicability to large volumes in industry might be limited.

In another study, Wiecinska *et al.* [101] used D-Galacturonic acid and Lactobionic acid, and reported one of the lowest viscosities (almost 1 Pa.s at a constant shear rate of 100 s^{-1}) even at 50 vol.% solids content. With such a low viscosity for such a high solids contents, one of the highest green densities in alumina nanopowder suspensions was reported. They reported relative densities of 68-69%. Rigorousness of the experimental steps should be noted. Fig.2.6 shows the experimental steps of this study. The effect of the meticulous experimental steps on the success of the particle packing cannot be underestimated. As a result of such a high green density, the sintered densities around 98% was reported.

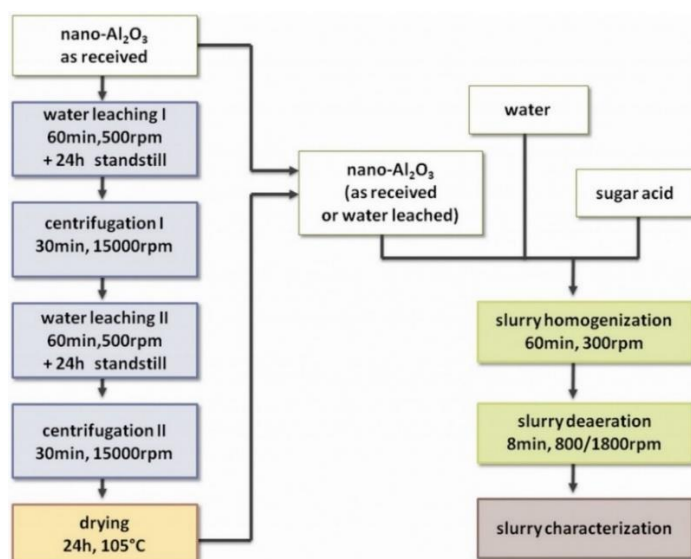


Figure 2.6. Schematical representation of experimental steps reported by Wiecinska *et al.* Retrieved from [101]

Çınar and Akinc [63] recently reported that commercially available ascorbic acid (Vitamin C) can be used to prepare highly loaded alumina nanopowder suspensions. They showed viscosity can be reduced up to 98% in aqueous suspensions of powders having average particle size of 42 nm. Fig.2.7 shows the effect of amount of ascorbic acid on the reduction of viscosity. Addition of ascorbic acid effectively reduced the viscosity of the alumina nanopowder suspension. Minimum viscosity point was reached at 1 wt.% ascorbic acid addition. It was also reported that transition in the flow characteristics from shear thinning to Newtonian behaviour was observed, which indicated a good dispersion. Further addition of the ascorbic acid resulted in increase in viscosity and shear thinning behaviour started to be observed again. From these results, it was concluded that addition of 1 wt.% ascorbic acid might be the point of monolayer coverage which meant further addition might result in bridging and depletion.[63] For all solids content, reduction in the viscosity was observed. Reduction rates was 98% and 94% for 20 and 30 vol.% solids contents while rate was decreased to 30% for 40 vol.% solids content, which was one of the highest viscosity reduction reported in the literature. It should also be noted that ascorbic acid is

commonly available dispersant and in this study, suspensions were prepared simply by conventional mixing.

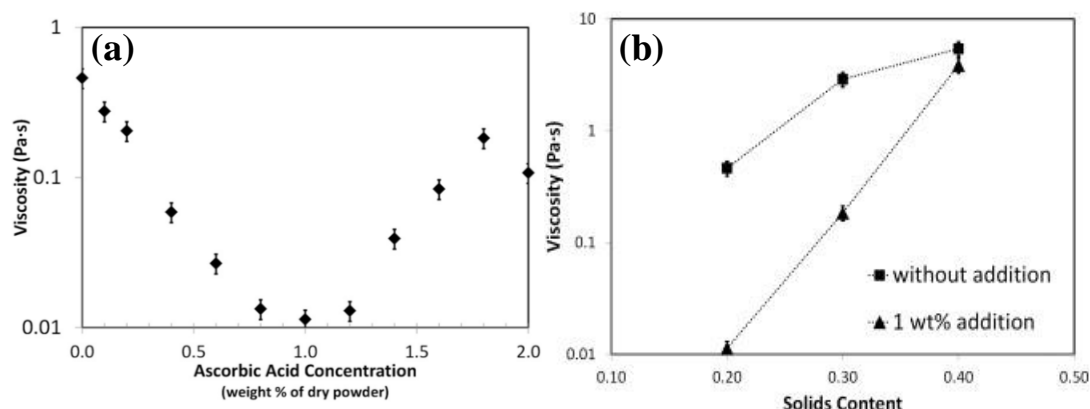


Figure 2.7. (a) Variation of viscosity of 20 vol.% nano alumina suspensions with different concentrations of ascorbic acid as a function of ascorbic acid concentration (b) Effect of ascorbic acid concentration of 1 wt.% on the viscosity as function of solids content at a constant shear rate of 100 s^{-1} . Retrieved from [63]

2.3. Sintering of the Alumina Ceramics

Sintering may result problems in atomic diffusion due to the presence of organic additives in structure during sintering. To overcome this problem, additive removal step is applied to green bodies before sintering. Studies have shown that temperatures ranging between 400-700 °C to burn organic additives for 1-2h would be the optimum time. [102–104]

In the sintering process many parameters should be controlled. Studies showed that the sintering technique, sintering temperature, heating rate and sintering time are the most important parameters for conventional sintering of alumina green bodies. [35,39–41,102–115] Maizza *et al.* [103] studied the effects of these different parameters on the sintered density and grain sizes. In this study, it was obtained that using higher temperatures will facilitate the densification process during sintering. Even though keeping sintering temperature as high as possible will provide the best result, the grain growth will be observed as a result of excessive sintering temperatures. In this context, studies conducted on the sintering of alumina ceramics have covered a wide range of temperatures from 1300 °C to 1700 °C.

[35,104,107,109,111,114] It was seen that 1300 °C was not enough to achieve fully dense structure, while 1700 °C was excessive and resulted in formation of large grains. Optimum sintering results were reported in the range between 1500 °C - 1600 °C to obtain of fully dense structure and the smallest grain size.

Sintering time was reported as another important parameter. [103] The densification curve as a function of sintering time given in Fig.2.8, three slopes for densification of samples were observed. In the first step, densification by 10-15% was observed. In the second step, major densification up to 90% and fast shrinkage was observed. In the last step, pores are mostly eliminated and final density was achieved. Besides, it can be seen that the sintering was completed in 20 mins. Although the exact time for sintering of green body will depend on a sample, excessive sintering times will result in excessive grain growth. When Fig.2.8 is further examined, it can also be seen that samples the grains of the samples sintered for 1 hour were coarsened by 1.5 times of the grain size of samples sintered for 20 min.

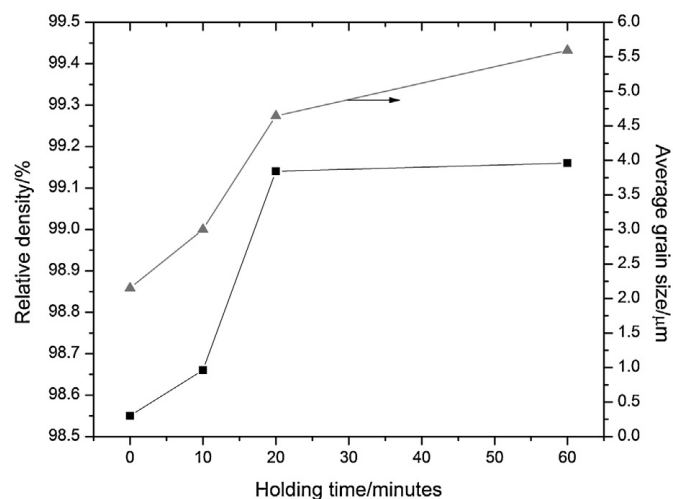


Figure 2.8. Effect of sintering time on relative densities and average grain sizes. Retrieved from [103]

Another and probably one of the most important parameters of sintering is the heating rate. Aminzare *et al.* [39] reported that application of higher heating rates resulted in lower final densities but smaller grains, whereas smaller heating rates resulted in

higher final densities but higher grain sizes. Importance of the heating rate was studied in a more detailed manner by Prajzler *et al.*[102] Heating rates ranging from 5 to 1500 °C/min was applied and decrease in final density down to 10% with increasing heating rate was reported. In the optimization of small grain sizes and high sintered density, applied heating rate is significant, otherwise expected densities may not be obtained.

Further studies on the effect of heating rate were also reported. [116–127] These studies were focused on the consideration of time or energy saving or mechanisms of densification. Applying a heating rate that will not generate thermal stress that can cause fractions in the green bodies and that will ensure that all chemical reactions have taken its place until the temperature sintering begins is a necessity. In order to reach higher densification with minimized grain growth, increasing the heating rate after reaching the temperature, at which sintering begins, to reach desired sintering temperature as fast as possible to minimize grain growth and achieve higher densification is maybe defined as the key parameter in the sintering process.

Apart from the importance of sintering parameters, the phase changes occurring during sintering is another critical issue in sintering of alumina nanopowders. Alumina nanopowders are either available in transition phases or aggregated α -phase. [128] Once the transition phase powder are used to obtain good dispersion properties, the volume change occurs due to phase change and introduce a new volume required to be filled by diffusion during sintering. This condition increases the required the sintering time and leads to increase in grain sizes. Transitional phases are also themodynamically stable phases in room temperature but phase transition to α -phase occurs since it is the most stable phase under high temperatures (1100 °C - 1200 °C) (Fig.2.9). Due to the density difference between α -Al₂O₃ (3.98 g/cm³) and γ/δ -Al₂O₃ ($\gamma/\delta \approx 70:30$, 3.67 g/cm³), volume shrinkage is calculated as 7.8 %. It was reported that this phase transition during sintering resulted in relatively low final (sintered) densities around 80-90% because of newly generated pores. [34,111]

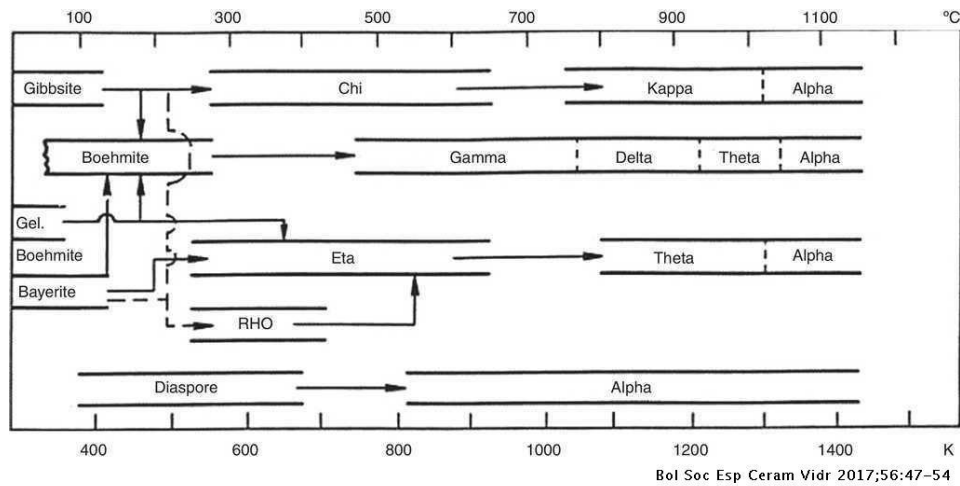


Figure 2.9. Phase transition diagram of Al₂O₃. Retrieved from [129]

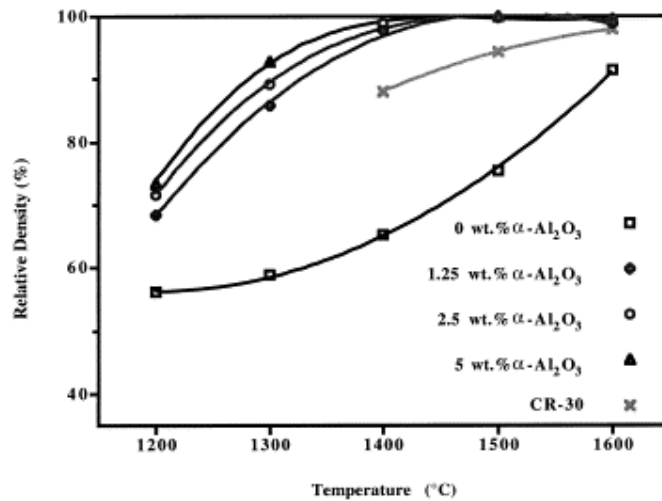


Figure 2.10. Sintered densities of α-seeded γ-Al₂O₃ and δ/α-Al₂O₃ samples with respect to seed amount as a function temperature. Retrieved from [109]

In open literature, different techniques were offered by researchers to reach fully dense structure even in the presence of phase transition. Examples include excessive temperatures [35], application of pressure [130], microwave sintering [131], sintering aids like addition of titanium [107] and seeding powders with α-phase of alumina powders. [109,110] When these techniques are compared, it was concluded that the seeding of α-phase of alumina powders would be the best choice in reaching best results under considerations like difficulty of the technique, cost, final grain size and final density. Interrelatedly, Fig.2.10 shows the results of final densities with or

without addition of α -phase seed powder. As it can be seen, seeded bodies achieved fully dense structures even in lower sintering temperatures while transition powder could not be densified more than 90%. These results was attributed to the increase in nucleation site densities of α -phase during phase transformation. [110]

CHAPTER 3

EXPERIMENTAL DETAILS

3.1. Materials

Alumina powder with high purity ($\geq 99.5\%$) (Lot number: AAGL 1201) and phase distribution of $\gamma/\delta \approx 70:30$ was purchased from Nanophase Technology Corporation (Burr Ridge, IL). The powder had a density of 3.67 g/cm^3 and BET specific surface area of $38.8 \text{ m}^2/\text{g}$. Its average particle size of 42 nm was calculated as its equivalent spherical particle diameter from BET specific surface area. All the other properties were reported in other studies. [44,63,132]

A commercially available alumina powder (Premalox 0.3 DA) from Ocean State Abrasives (West Warwick, RI) was purchased and used as α seed. The powder had a density of 3.98 g/cm^3 and was in fully α -phase. TEM micrographs of the alumina nanopowder and SEM micrograph of seed were given in Fig.3.1.

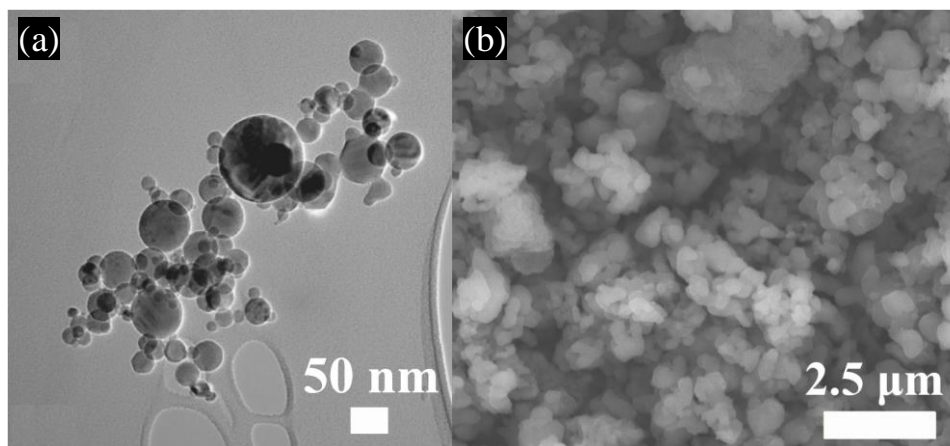


Figure 3.1. (a) TEM micrograph of alumina nanopowder (b) SEM micrograph of seed α - Al_2O_3 powder

NaCl (ACS certified) from Fisher Scientific (Fair Lawn, NJ) and D-fructose (99%) from Alfa Aesar (Lancashire, UK) were purchased. L-(+)-ascorbic acid (ACS certified), having a purity of 99%, was purchased from Alfa Aesar (Ward Hill, MA). Ultrapure water with the resistivity of 18.2 M Ω cm was used for all suspensions.

3.2. Experimental Methods

3.2.1. Preparation of Suspensions

3.2.1.1. Preparation of Suspensions with Fructose and NaCl

Alumina powder was dried at 110 °C for 2h prior to experiments. NaCl and D-fructose were added to the ultrapure water, and solution was magnetically stirred to reach high homogeneity for 30 min. prior to addition of alumina powder. Required amounts of NaCl were estimated in molar quantity of solution and different molarities were studied. However, required amount of D-Fructose was determined directly from the results reported by Çınar and Akinc [49] and fructose which was 4 weight percent of the alumina powder in suspension. The density of the fructose was taken as 1.69 g/cm³ and volume of the added fructose was taken into account to maintain volume percent of solids in suspensions and to calculate the required amount of water accurately. Once fructose and NaCl was dissolved in water, alumina powder as a volume percentage of the suspension was slowly and carefully added into the solution. For instance, to prepare 10 mL of this particular suspension, 7.34 g ($2 \text{ mL} \times 3.67 \text{ g/cm}^3 = 7.34 \text{ g}$) nano alumina powder (which was dried at 110°C for 2 h prior to weighing), and 0.294 g fructose (4 wt.% of alumina) were weighed separately. Fructose was then added to the sufficient amount of ultrapure water ($8 \text{ mL} - (0.294 \text{ g per } 1.69 \text{ g/cm}^3) = 7.83 \text{ mL H}_2\text{O}$) to make 8 mL of fructose solution to which the alumina powder is then added slowly. Solids content represented as a volume fraction of the alumina powder with respect the volume of total suspension.

Prepared suspensions were magnetically stirred at 1000 rpm for 24h at room temperature prior to slip casting to reach high homogeneity and consistency in results.

In studies where the seed α -Al₂O₃ powder was used, the amount of seed powder was measured as a weight percentage of the alumina nanopowder and added to the suspension together with alumina nanopowder. The density of the seed alumina was taken as 3.98 g/cm³ and volume of the seed powder was taken into account in sample preparation.

3.2.1.2. Preparation of Suspensions with Ascorbic Acid

Alumina powder was dried at 110 °C for 2h prior to experiments for removal of moisture. 1 wt.% of ascorbic acid addition with respect to the powder amount was used to obtain minimum viscosity. [63] The required amount of ascorbic acid was first dissolved in ultra pure water by stirring for 30 min. Volume of the ascorbic acid in suspension was not taken into account since the added amount was negligible.

Alumina nanopowder was measured as volume percentage of the suspension and slowly added to the solution. Solids content represents the volume fraction of the alumina powder with respect the total suspension. Prepared suspensions were magnetically stirred at 1000 rpm for 24h at room temperature prior to slip casting.

In experiments where the seed was used, procedure was completely same with the procedure described in preparation of suspensions with fructose and NaCl.

3.2.2. Slip Casting and Sintering of Alumina Bodies

The suspensions were slip casted into cylindrical polymeric molds (12.5 mm diameter, 7.5 mm thickness) which was placed on a plaster of paris to facilitate the drying process by providing suction of water from bottom of the system while evaporation was provided from top of the system. The casted suspensions were left to dry for 24h in room conditions. Then, the samples were kept in a dessicator for another 24h.

Dried green bodies of alumina were put into furnace and heated to 550 °C with a heating rate of 5 °C/min and kept at that temperature for an hour to remove organic contents. Then, bodies were further heated to 1000 °C with the same heating rate again. After reaching 1000 °C, heating rate was increased to 10 °C/min to minimize

the grain growth. No isothermal hold was applied during heating rate change and samples were heated up to 1600 °C and kept at that temperature for 2h. After finishing sintering step ends, samples were left in the furnace to cool down to room temperature.

3.3. Characterization of Green and Sintered Bodies

3.3.1. Green and Sintered Density Measurements

Archimede's method was used to measure the relative densities of green and sintered alumina bodies. In this method, green and sintered bodies were weighed first as dry then weighed bodies which were immersed into paraffin oil and allowed paraffin oil to fill pore cavities then taken out from liquid and they were called saturated bodies. Lastly, saturated bodies were weighed in paraffin oil and they were called saturated suspended bodies. For saturation, samples were kept for 5 minutes in paraffin oil. The density of paraffin oil was determined as 0.762 g/cm³. To calculate green and sintered densities, used equations are given as follows:

$$V_{\text{Bulk}} = \frac{W_{\text{Saturated}} - W_{\text{Saturated Suspended}}}{\rho_{\text{Paraffin Oil}}} \quad (3.1)$$

$$\rho_{\text{Density}} = \frac{W_{\text{Dry}}}{V_{\text{Bulk}}} \quad (3.2)$$

$$\text{Green Density} = \frac{\rho}{3.67 \frac{\text{g}}{\text{cm}^3}} \times 100 \quad (3.3)$$

$$\text{Sintered Density} = \frac{\rho}{3.98 \frac{\text{g}}{\text{cm}^3}} \times 100 \quad (3.4)$$

where V is the volume, W is the weight and ρ is the density.

In order to calculate error margin, three different suspensions were prepared and three different samples were slip-cast from each suspension. The average of 9 samples was presented as the result. The error margins were determined from the maximum and minimum values obtained from measurements.

3.3.2. Rheology Measurements

The measurements were done with a rheometer (model AR 2000ex, TA Instruments, New Castle, DE) and a measuring cone having angle of 4° and diameter of 40 mm was used during measurements. Solvent trap was used to prevent evaporation of water in the suspension. Applied shear rate was firstly increased from 0.5 s^{-1} to 500 s^{-1} and decreased back to 0.5 s^{-1} . For accuracy, 2 consecutive cycles of shear rate were measured with 20 points for each cycles at $25^\circ \pm 0.1 \text{ }^\circ\text{C}$. The data of the final half loop was given during the thesis.

3.3.3. Scanning Electron Microscopy

During SEM characterization, a field emission scanning electron microscope (FE-SEM) (FEI Nova NanoSEM 430) at a voltage of 20 kV was used and the morphology of the nanoparticles, green and sintered bodies were examined. Before the FE-SEM analysis, surface of the samples were coated with gold by Polaron SC 7640 Sputter Coater to provide conductivity.

The average size of grain boundaries was estimated by the linear intercept method using SEM images.

CHAPTER 4

COMBINED EFFECT OF FRUCTOSE AND SODIUM CHLORIDE ON PARTICLE PACKING AND SINTERING BEHAVIOURS

4.1. Particle Packing Behaviour

Dispersion behavior of particles in suspension strongly affects the packing behavior of particles when consolidated. In order to obtain high packing efficiency, repulsive forces between particles should be strong enough to prevent agglomeration during consolidation. Moreover, there should be enough free space and time for movement of particles in such a way that particles can re-arrange themselves to find lowest energy positions and ends up with random close packing structures. [36,133,134]

The effect of fructose and NaCl addition on the packing behavior of highly loaded alumina nanopowder suspensions is illustrated in Fig. 4.1. Without any additives, hydration and electrical double layers form around alumina powders in aqueous suspensions. Due to the large space occupied by these layers, particles cannot move freely in suspensions, therefore loosely packed structures are obtained when consolidated. Fructose added in aqueous alumina suspensions interacts with alumina surface and replace the bound water. [48] Therefore, the amount of free water increases in fructose added aqueous alumina suspensions. NaCl, on the other hand, is known as indifferent electrolyte for alumina, but can effectively shrink the electric double layer formed around particles. As a result, significant free space is provided for particle movement. With use of optimum amount of NaCl, the electrostatic repulsive forces between particles can be preserved, therefore agglomeration tendency during consolidation is also minimized. Similarly, fructose molecules around particles prevent agglomeration due to their physical presence. When both fructose and NaCl is used, closely packed alumina green bodies can be obtained.

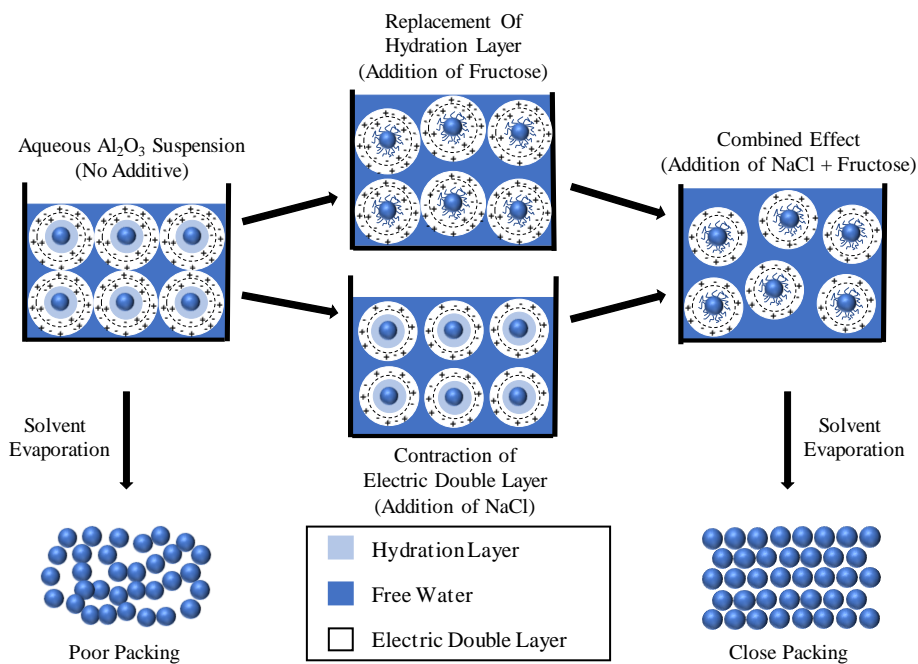


Figure 4.1. Schematical comparison of no additive and combined effect on the initial particle packing produced from aqueous alumina nanopowder suspensions. Addition of fructose and NaCl contracts hydration and electric double layers which increases available interparticle spacings. Increased interparticle spacings results in close packing compared to its counterpart with insufficient interparticle spacing.

As discussed in literature, inter-particle spacing dominates the rheological behaviour of suspensions, which, in turn, controls the particle packing behaviour. Besides, addition of fructose and NaCl affects the available space between particles. In order to estimate the availability of IPS and its relation to suspension viscosity and packing behaviour, IPS values were calculated. First Funk and Dinger's relation (Eq. 2.6) was used. When particle size is taken as monodisperse size of 42 nm and inserted in to Eq.(2.6,) IPS values are calculated as 48.1 nm, 24.8 nm and 13.1 nm for 0.20, 0.30, and 0.40 solids contents respectively. In these calculations, conventional mixing was used, so maximum packing was considered as 0.64 and particles were assumed to be hard spheres. These values can be explanatory when compared with interparticle spacing between 1 μm sized particles. (Table 4.1)

Table 4.1. *IPS estimations for alumina nano and micron sized powders in aqueous media.*

Solids Content	<i>IPS (D:42 nm)</i>	<i>IPS (D:1 μm)</i>
0.20	48.1 nm	1146 nm
0.30	24.8 nm	590 nm
0.40	13.1 nm	312 nm

The distance between two particles having 1 μm are calculated as 1146 nm, 590 nm and 312 nm for 0.20, 0.30, 0.40 solids content, respectively. It can be realized that the distance between the particles diminishes significantly when nanopowders are used. As a result, it is expected that particles will interact more with each other and the flow of suspension will be difficult, thus the viscosity of suspensions is expected to increase. Therefore processing of nanopowder suspensions are challenging.

In order to estimate the available IPS for aqueous nanopowder suspensions (IPS_{aq}), the presence of the hydration layer (HL) and the electric double layer (EDL) should be taken into account. To do this, Kuwabara's virtual cell was used as shown in Figure 4.2. Firlar *et al.* [54] directly observed alumina nanopowders in aqueous media by fluid cell STEM and showed that the hydration layer present around powders more like a nonuniformly distributed clouds showing that the powders were in an agglomerated form. In this study, in order to estimate the average ΔR_{HL} , it was assumed that the bound water content around the particles was uniformly distributed and formed homogeneous layer around particles as illustrated in Figure 4.2.

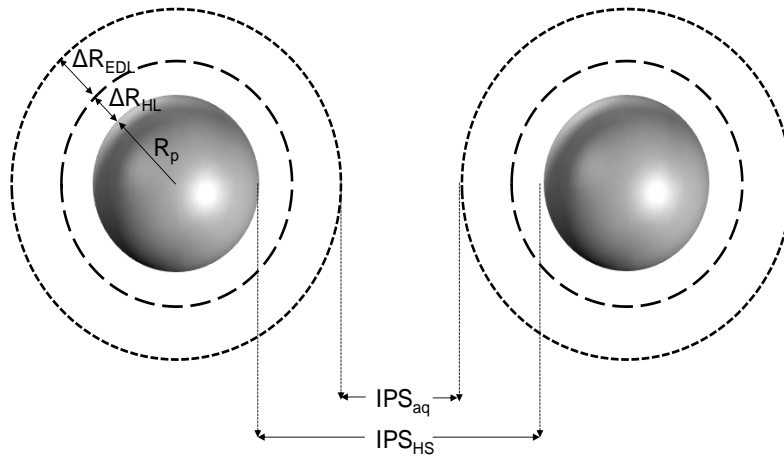


Figure 4.2. Kuwabara's virtual cell was modified in order to account for the effects of electric double layer and the hydration layer. IPS_{HS} is the inter-particle distance with hard-sphere assumption; IPS_{aq} is the inter-particle distance in aqueous solutions. R_p is the radius of particles, ΔR_{EDL} is the Debye length, and ΔR_{HL} is the hydration layer thickness.

In order to reveal the effect of electric double layer and hydration layer in available interparticle spacing, the thickness of both layers were estimated. Electric double layer thickness was computed using Eq.(2.3). In the absence of NaCl, the electric double layer thickness would be too large and cannot be calculated. In order to account for the ions present in solution due to impurities and slight solubility of alumina, The ion concentration was taken very low (0.001 M) and its behavior is assumed like monovalent ion.

For hydration layer calculations, bound water was assumed to be evenly distributed between particles and as homogeneous layers as it was shown in Fig.4.2. In order to estimate the average ΔR_{HL} , we assumed that the bound water content was evenly distributed between monodispersed individual particles and formed homogeneous layer around particles as illustrated in Figure 1. Cinar and Akinc previously reported the bound water layer content for aqueous suspensions of similar alumina nanopowder. For calculations, the data presented in previous studies was used. [49,50,54]. For example, for calculation of hydration layer, bound water weight fraction was given as 0.28 at 0.20 solids content [49] and the density of bound water is assumed 1 g/cm^3 . Therefore, the volume fraction of bound water is 28% of the total

water content, which is equal to 22.4% of the total volume ($\frac{8 \text{ mL water} \times 0.28}{10 \text{ mL suspension}} = 0.224$).

Since the bound water will act as a part of particle and cannot serve as solvent, the effective volume fraction (Φ_{eff}) can be considered as 0.424 according to the Eq.(2.10). From Φ_{eff} , the hydration layer thickness (ΔR_{HL}) can be calculated as 6 nm according to the Eq.(2.11) for particles having size of 42 nm.

The estimated average interparticle spacing values calculated for various solids content were presented in Table 4.2.

Table 4.2. Comparative estimations of IPS and available IPS under the effect of HL and EDL with respect to solids content in the absence of NaCl.

Φ	IPS_{HS} (nm)	ΔR_{HL} (nm)	ΔR_{EDL} (nm) [NaCl]: 0.001 M	IPS_{aq} (nm)
0.20	48.1	6.0	9.6	16.9
0.30	24.8	5.7	9.6	-5.8
0.40	13.1	5.2	9.6	-16.5

Depending on the calculated results given on Table 4.2, IPS decreased from 48 nm to 17 nm, 25 nm to -6 nm and 13 nm to -17 nm for 0.20, 0.30 and 0.40 solids contents respectively. For a system having a powder size of 500 nm, these values can be obtained at solids loading of 0.60. However, when solids content was increased to 0.30 or 0.40, IPS was found to be negative, which indicated that the hydration and electric double layers overlapped. Therefore, it could be concluded that this suspension would lead to agglomeration which would obstruct particle rearrangement during slip casting.

As it was discussed in literature, one could try to shrink HL and EDL by additions of fructose and NaCl to increase the available IPS_{aq} . Calculated values of the available IPS_{aq} after additions of 4 wt.% fructose and 0.01 M NaCl can be seen on Table 4.3.

Table 4.3. Comparative estimations of IPS and available IPS under the effect of HL and EDL with respect to solids content.

Φ	IPS_{HS} (nm)	ΔR_{HL} (nm)	ΔR_{EDL} (nm) [NaCl]: 0.01 M	IPS_{aq} (nm)
0.20	48.1	4.3	3.0	33.5
0.30	24.8	3.6	3.0	11.6
0.40	13.1	3.2	3.0	0.7

One of the important observation from these calculations is that the thicknesses of hydration layer was reduced to less than three-fourth of the initial thickness with the presence of fructose molecules in the system. Moreover, EDL was decreased to one-third of the initial thickness and available IPS values were increased for all solids content. It was also calculated that available IPS became positive value at solids content of 0.40.

In the literature section that individual and combined effects of hydration and electric double layer on rheological behavior of nanopowder suspensions were reported before. [7,44,49,132,135] In order to improve these understandings and effect of IPS on particle packing behaviour and in order to investigate the compatibility of these calculations with experimental results, viscosity of the suspensions in different solids contents measured before and after increasing the IPS by modification of the layers. Measurements and its effects on the green density was given in Fig.4.3. It was observed that viscosity could be decreased for all solids content, when the available IPS was increased. Rheology measurements were also fit into power law model given in Eq.(4.1) and presented in Table 4.4.

$$\sigma = K \times \gamma^n \quad (4.1)$$

where σ is shear stress, K is flow consistency index, γ is shear rate and n is power law index.

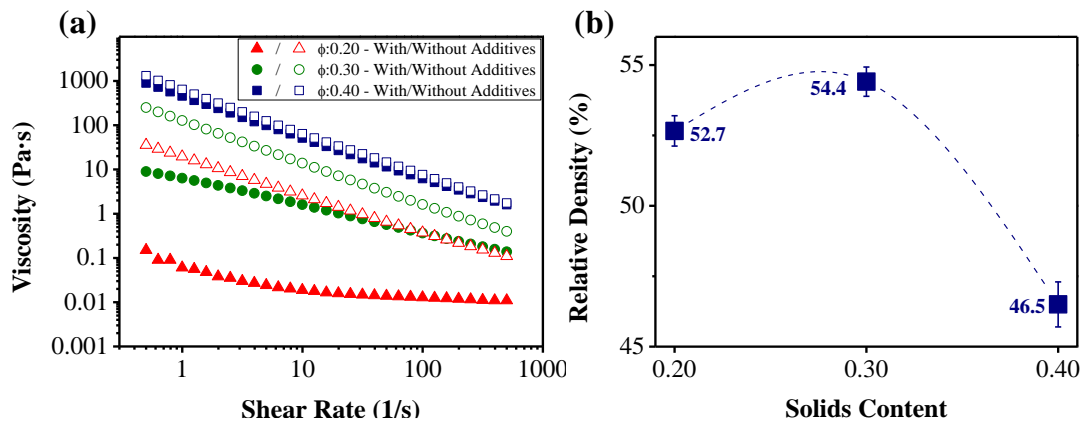


Figure 4.3. (a) Change in viscosity with respect to solids content as a function of shear rate and (b) its effects on initial particle packing density

*(All suspensions constantly have 4 wt.% Fructose and 0.01 M NaCl concentration.)

Table 4.4. The power law parameters obtained from the rheological behavior of alumina nanopowder suspensions. As additives 4 wt% fructose and 0.01M NaCl were used.

Φ	<i>no additive</i>		<i>with additives</i>		<i>The change in K with additives</i>
	<i>K</i>	<i>n</i>	<i>K</i>	<i>n</i>	
0.20	18.763	0.155	0.0533	0.684	- 99.7%
0.30	124.17	0.062	0.4971	0.379	-94.9%
0.40	613.66	0.047	442.5	0.079	-27.9%

Power Law: $\eta = K \cdot \dot{\gamma}^{n-1}$, where η is the suspension viscosity, K is the consistency coefficient and n is the power law index. R^2 for fitting of the rheological behavior of suspension with solids content of 0.20 with additives is 0.85, for others the value is larger than 0.999.

The consistency index (K) in power law is the indicator of the level of the viscosity over the range of applied shear rate. As realized in Table 4.4, the viscosity of suspensions reduced with addition of fructose and NaCl regardless from the solids content of suspension. Yet, the effect of fructose and NaCl addition was diminished

as the solids content increased. While the consistency index could be reduced by almost 100% for solids loading of 0.20, the reduction on this value was about 95% and 28% for solids loading of 0.30 and 0.40, respectively. Considering very high initial viscosities, such a reduction was enough to obtain significant fluidity. In the power law, K indicates the extent of viscosity, while n is a power law index. The power law index (n) shows the level of shear thinning behavior of suspensions such that the values close to 0 indicates a significant shear thinning behavior while the values approaches to 1 indicates a Newtonian flow behavior. As shown in Table 4.4, addition of fructose and NaCl to suspensions with solids content of 0.20 led to significant change in flow behavior from strong shear thinning character ($n:0.155$) to less shear rate independent Newtonian flow ($n:0.684$) indicating that that the effect of attractive interparticle interactions were minimized. For higher solids content, the power law index increased and severe shear thinning behavior was observed. Regardless from the solids loading, the power law index decreased with addition of fructose and NaCl indicating more homogeneously dispersed stabilized suspensions.

Consistently, green densities over 50% could be observed and slight increase in density was observed (52.7% to 54.4%). However, the power law index of suspensions at 0.40 solids content supported the calculation showing that it had too small IPS value to allow free movement of particles. As a result, no remarkable decrease in viscosity could be achieved and green density could not exceed 50% (46.5%). This phenomenon could be attributed to the absence of sufficient IPS for new incoming particles to place on energetically low positions and disruption in the searching ability of particles to find these low energy positions. [36,133,134] Besides, less time is allowed for particles for searching due to the higher attractive interaction between particles arising from the reducing interparticle spacing between particles.

Further investigation was done on the effects of increased IPS by modified layers on the micrographs showing the particle packing structure of the green bodies at macro-micro-nano scale and it can be seen on Fig.4.4. In consistency with high green density results of samples having 0.20 solids content, surface with high smoothness and no

porosity was observed on its macro and micro structure (Fig.4.4 (a,b)). Particle packing structure was also in line with the observations done in macro and micro states of the green body (Fig.4.4 (c)). When the solids content was increased to 0.30, slightly reduced smoothness of the surface was observed due to the increased viscosity (Fig.4.4 (d,e)) but there was still no observable porosity. When the nano-scale of the samples were investigated (Fig.4.4 (f)), efficient packing with homogeneous structure obtained in 0.20 solids content was replaced with the slightly disrupted homogeneity for 0.30 solids content.

With the further increase in solids content, large pores, which can be observed even with bare eyes, appeared on the surface of samples (Fig.4.4 (g)). Similar results were obtained in the microstructures of the samples (Fig.4.4 (h)) and porosity with loose packing was present even in the nanostructure of the samples (Fig.4.4 (i)), which was an clear indicator that particles could not re-organize their positions to the lowest energy spots due to the insufficiency of the available IPS.

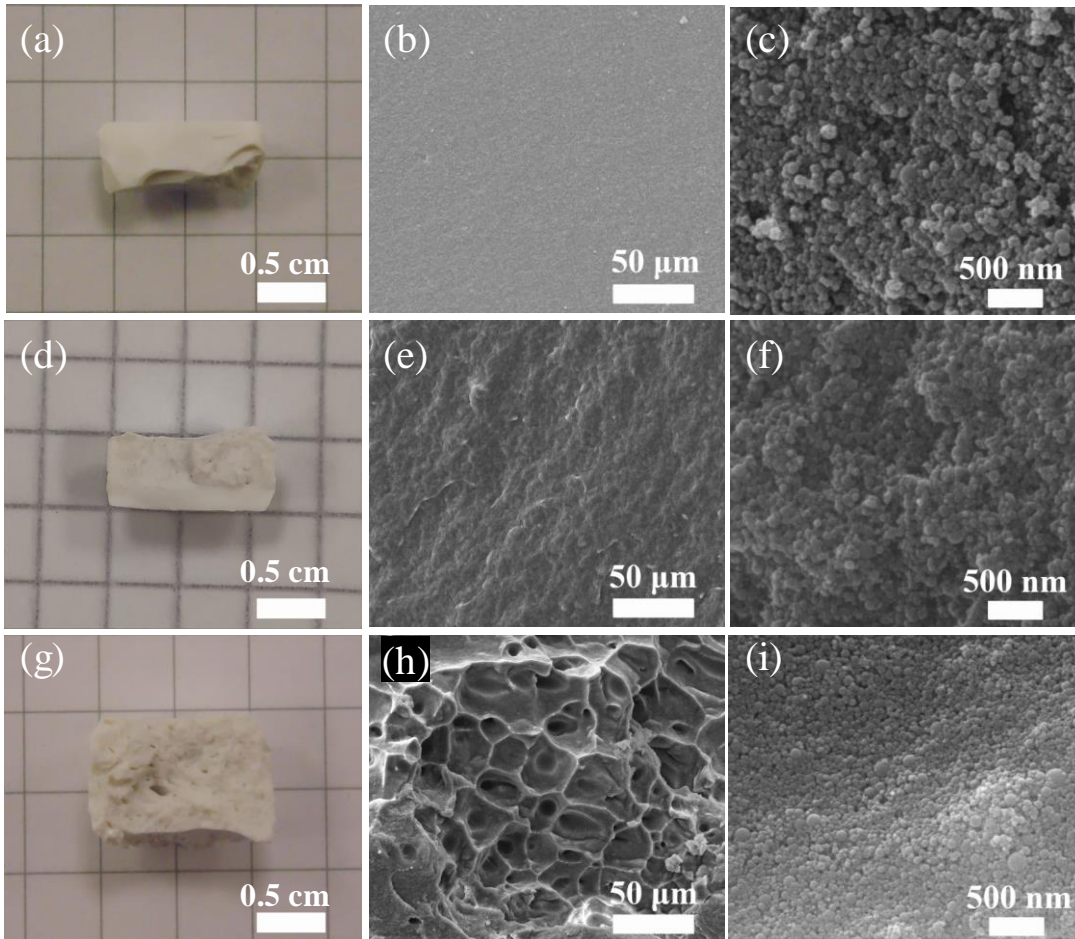


Figure 4.4. Effect of contraction of hydration and electric double layers on particle packing behaviour at (a-c) 0.20, (d-f) 0.30, (g-i) 0.40 solids content and their macro-micro-nano structures are given from left to right respectively.

From all the results and discussions above, it could be easily concluded that providing additional interparticle spacing was terminally significant in order to improve the initial particle packing behaviour of samples having 0.40 solids content by further contraction of hydration and electric double layers. Even though the further contraction in the hydration layer could not be tested hydration layer as it was constant for particle size and solids content, further contraction in the electric double layer could be provided by increasing the concentration of the NaCl in the suspension in order to achieve further reduction in the viscosity. Here it should be noted that keeping the net interaction energy between particles in repulsive region even after contraction

electric double layer was a necessity to maintain the repulsive ability for lower viscosity. Hence, net interaction energy between particles should have been carefully considered and taken into account for the maintaining the stability of the suspension while more IPS was also provided by contraction of electric double layer. Interestingly, it was shown that zeta potential values of alumina nanopowder in aqueous solution was reported to increase with addition of very small amount of NaCl. [44] However, zeta potential values were reported to decrease at higher NaCl concentrations. Empirical calculations on the decrease of Debye Length by using Eq.(2.3) and its effect on the net interaction energy between particles from DLVO curves with respect to different NaCl concentrations was calculated inserting reported zeta potential values into Hamaker software. [44,136] Results can be seen on Fig.4.5. Depending on these results, calculated IPS values is given in Table 4.5.

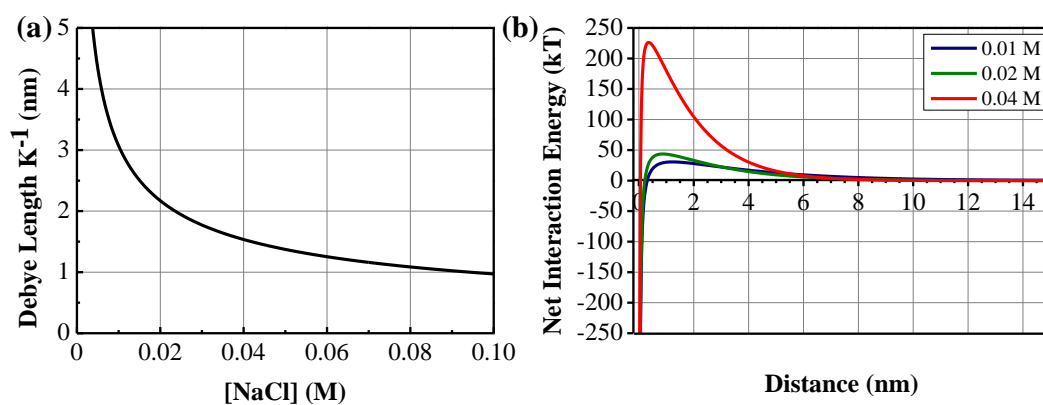


Figure 4.5. (a) Change in Debye Length (K^{-1}) with NaCl concentration and (b) its effect on Net Interaction Energy between particles as a function of distance

Table 4.5. The inter-particle spacing estimations for alumina nanopowders in aqueous solutions (IPS_{aq}). The effect of NaCl concentration were considered for suspensions with solids loading of 0.40 and with fructose addition of 4 wt%. For these suspensions, IPS_{HS} and ΔR_{HL} were estimated as 13.1 nm and 3.2 nm, respectively.

[NaCl]	ΔR_{EDL} (nm)	IPS_{aq} (nm)	<i>Power Law Model</i>	
			<i>K</i>	<i>n</i>
0.01 M	3.0	0.7 nm	442.5	0.079
0.02 M	2.1	2.5 nm	460.76	0.104
0.04 M	1.5	3.7 nm	93.824	0.192

As it was tabulated in Table 4.5, calculations have shown that Debye Length decreased from 3.0 nm to 2.1 and 1.5 nm when the NaCl concentration is increased from 0.01 M to 0.02 and 0.04 M respectively. It was found that the available IPS was increased to 2.5 nm and 3.7 nm when the NaCl concentration was increased to 0.02 M and 0.04 M respectively. Consistently, viscosity measurements showed that n values went through higher values, which indicated better dispersion. For these NaCl concentrations, results of rheology and green density measurements can be seen on Fig.4.6.

In consistency with the set of data given in the Fig.4.5 and Table 4.5, effective reduction in the viscosity was obtained at the NaCl concentration of 0.04 M even though no noteworthy reduction could be achieved at 0.02 M (Fig.4.6 (a)). Reduction in the viscosity was calculated as 3-fold when the NaCl concentration is increased from 0.01 M to 0.04 M at a constant shear rate of 100 s^{-1} . Relatedly, promising changes in the green density Fig.4.6 (b) was obtained in the 0.04 M NaCl concentration although green density could not be noticeably increased due to the not effective reduction in the viscosity at 0.02 M NaCl, which clearly indicated that particles had gained enough spacing to move and place freely. As a result, green density could be increased up to 52.3% from 46.5%.

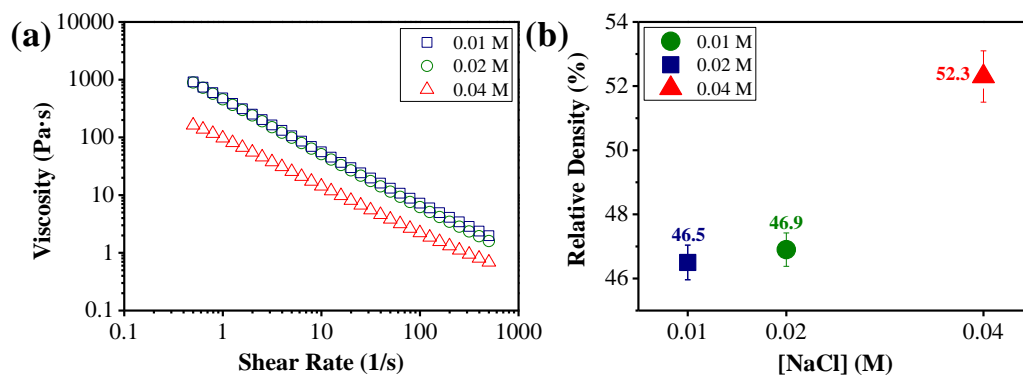


Figure 4.6. (a) Change in the viscosity with increasing NaCl concentration as a function of shear rate and (b) its effect on the initial particle packing density

*(All suspensions constantly have 4 wt.% fructose concentration and 0.40 solids content.)

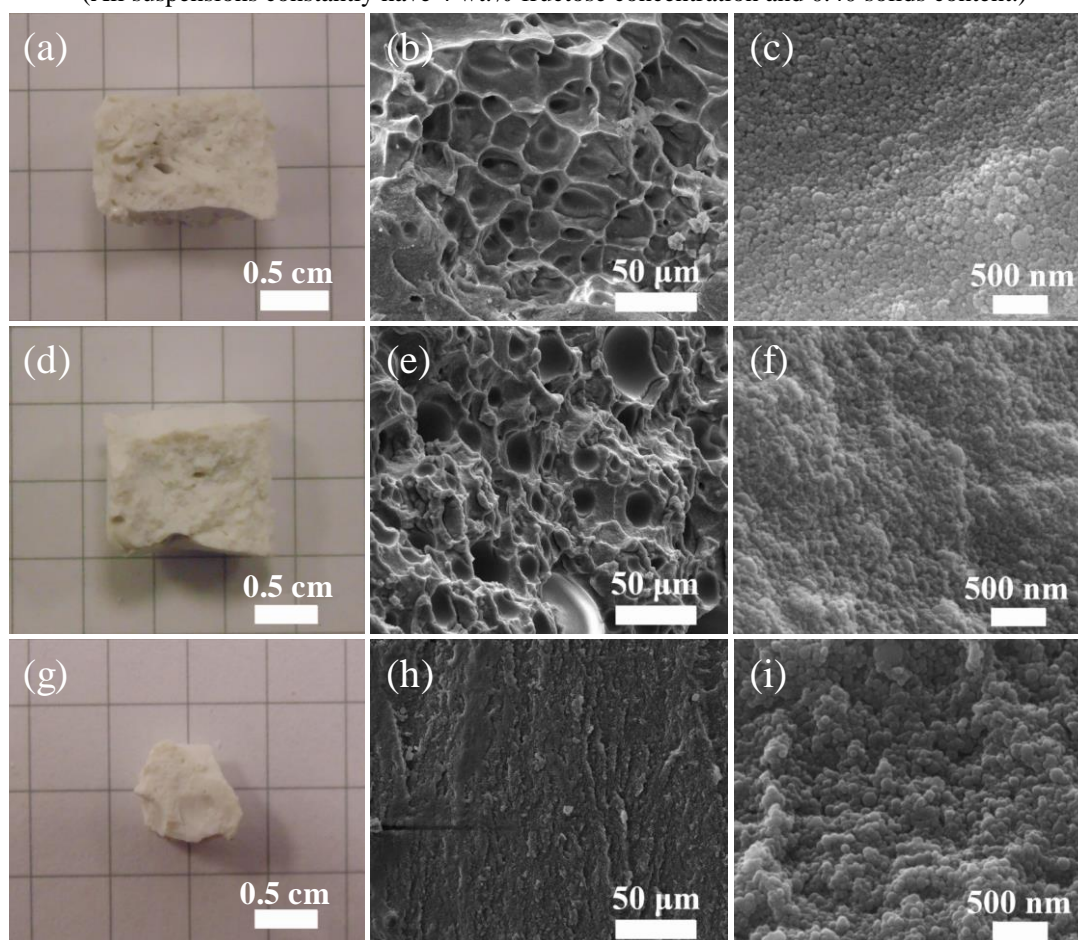


Figure 4.7. Evolution of microstructure and packing behaviour at 0.40 solids content with increasing NaCl concentrations of (a-c) 0.01 M, (d-f) 0.02 M, (g-i) 0.04 M and their macro-micro-nano structures are given from left to right respectively.

Effects of further contraction in the electric double layer on initial particle packing behaviour can be seen on the micrographs of samples given in the Fig.4.7. Interestingly, smaller and less interconnected pore structure was observed at 0.02 M (Fig.4.7 (d,e)) compared to macro and microstructures of samples at 0.01 M NaCl concentration (Fig.4.7 (a,b)). At the 0.04 M NaCl concentration, even smoother surface and no interconnection in the pore structure and less porosity was obtained (Fig.4.7 (g,h)). In the nanoscale, it was observed that the open pores between particles got smaller at 0.02 M (Fig.4.7 (f)) and disappeared at 0.04 M NaCl concentration (Fig.4.7 (i)). When the nanostructures of green bodies having similar green densities (samples having solids contents of 0.20, 0.30 at 0.01 M NaCl and 0.40 at 0.04 M NaCl) were compared, an interesting difference between them arises. It can be clearly seen on Fig.4.4 (c,f) and Fig.4.7 (i) that homogeneity in particle packing structure was replaced with firm and agglomerated packing structure with higher solids contents. In this context, Michálková *et al.* [137] studied dilute and concentrated systems and reported even higher green densities at highly concentrated suspensions than dilute systems. They related these results with the placement of strong agglomerations, which started to appear with increasing solids contents, into the pore cavities and it resulted in higher green densities. However, sintered results were lower than the sintered densities of dilute suspensions having lower green densities, since the strong agglomerations in the particle packing generated new pores and restrained the sintering process. Having lower sintered density results, when produced from high viscosities compared to the ones produced from low viscosities, was also reported by the Tallon *et al.*, even though the green densities were similar,. [34] Therefore, it can be concluded that even higher green densities are a requirement to achieve a fully sintered body from a green body which has high solids loading compared to their dilute counterparts having similar green densities. All in all, it can be expected that the green bodies having a solids content of 0.40 at 0.04 M NaCl concentration would not be able to reach the sintered densities that would be achieved with green bodies having solids contents of 0.20 and 0.30 at 0.01 M NaCl concentration.

4.2. Sintering Behaviour

To reveal the effect of packing structure on final density, all green bodies were sintered at 1600 °C for 2 hours. Depending on the sintering results of green bodies given in the Fig.4.8, it can be concluded that the interpretations depending on the viscosity, green density and the initial particle packing behaviour was consistent with the sintered density results. This clearly explains without leaving room for doubt why the highest sintered density result (95.7% of the theoretical density of α -Al₂O₃) was achieved at the solids content of 0.20. The volume change of alumina from γ - θ phase to α -phase of Al₂O₃ during sintering corresponds to about 8.4% shrinkage. The actual densities for the solids loading of 0.20 were compared, the green density of 1.93 g/cm³ was increased to the final density of 3.92 g/cm³ (Fig. 4.8). When this additional volume change occurring in sintering was considered, being able to increase the final density to such high levels with conventional shaping and sintering procedures could be attributed to the homogeneous distribution of small pores, hence to the efficient packing behavior. However, the sintered densities of 95.7% at 0.20 solids content and 93.4% at 0.30 solids content were one of the highest final density results for such a straightforward, easy and cheap production method.

Apart from these, the result for the samples having 0.40 solids content at 0.01 M NaCl concentration was expectedly low (66.2%). Increasing the NaCl concentration to 0.02 M could only slightly improve the sintering results (67.0%). This was also an expectable result since the packing behaviour of particle during drying could not be noticeably improved. However, green bodies could be sintered up to 76.2% when the concentration was 0.04 M.

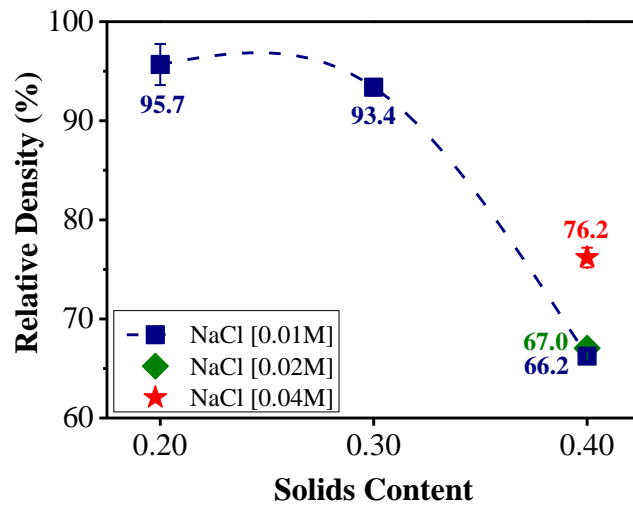


Figure 4.8. Effect of solids content and NaCl concentration on the sintered densities

Yet, it could not be sintered over relative densities of 90% at 0.40 solids content as solids contents of 0.20 and 0.30 even though they had similar green densities because strong agglomerations produced new pores during the sintering process. Effect of these results on the microstructure and average grain sizes can be seen on Fig.4.9 and Table 4.6 respectively.

Table 4.6. Effect of solids content and NaCl concentration on grain size.

Parameters [Solids content – NaCl Concentration]	Intercept Length (μm)
0.20 – 0.01 M NaCl	1.28
0.30 – 0.01 M NaCl	1.27
0.40 – 0.01 M NaCl	1.44
0.40 – 0.02 M NaCl	1.45
0.40 – 0.04 M NaCl	1.45

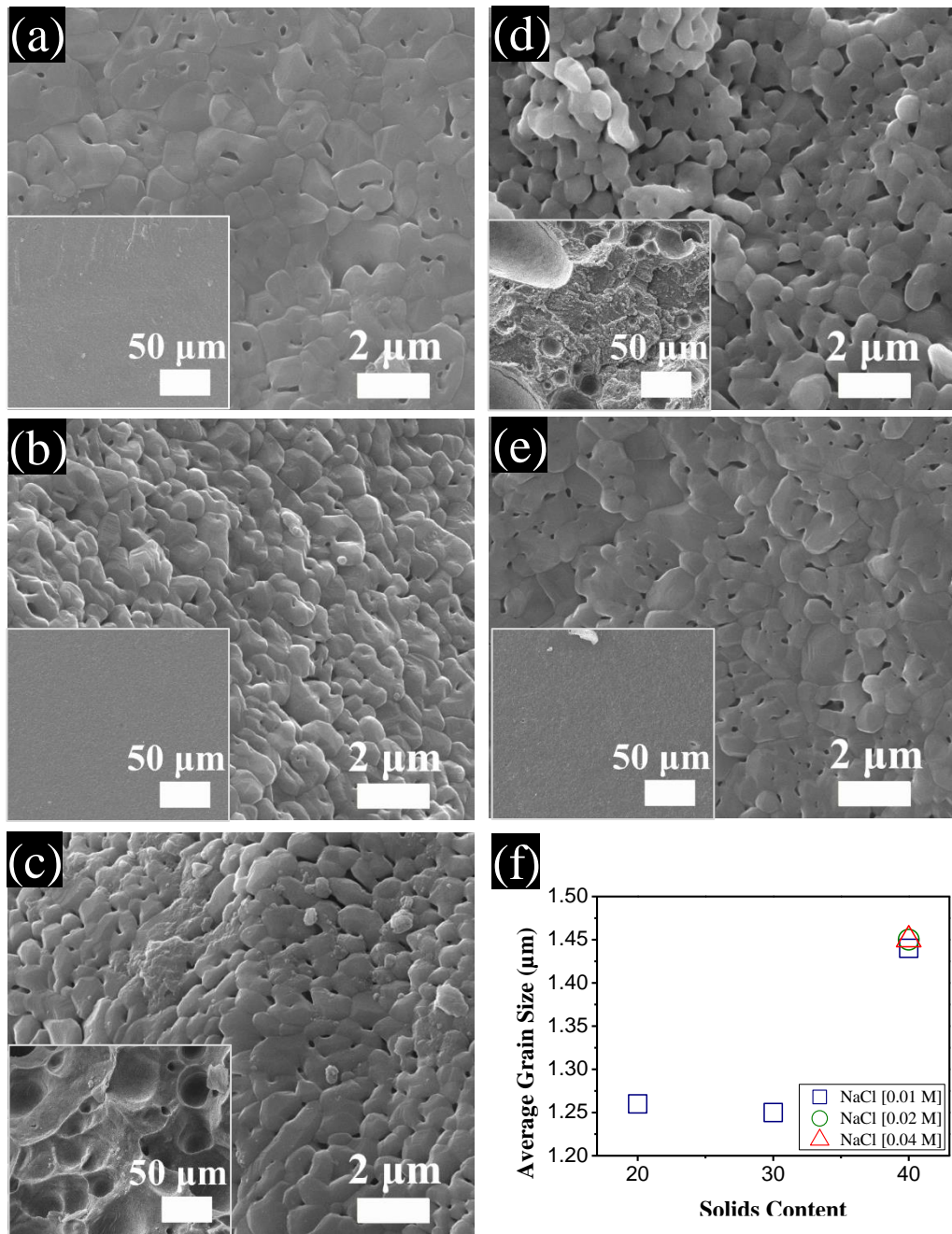


Figure 4.9. Effect of solids content and NaCl concentration on the microstructural evolution of sintered Al_2O_3 bodies. Sintered bodies are given as (a) 0.20 – 0.01 M NaCl, (b) 0.30 – 0.01 M NaCl, (c) 0.40 – 0.01 M NaCl, (d) 0.40 – 0.02 M NaCl (e) 0.40 – 0.04 M NaCl, (f) Average grain sizes as a function of solids content.

Microstructures of sintered samples was consistent with the sintered density results. Samples with 0.20 solids content was almost poreless in the microstructure and its grain size was estimated as 1.28 μm . Congruently, samples having solids content of 0.30 also showed almost no porosity but their measured average grain size was smaller (1.25 μm). Unfortunately, observable porosity was still present in the microstructure of the sintered samples having solids content of 0.40 and it could not be fully removed even with further increase in the NaCl concentration. When the sintered density results given in Fig.4.8 are considered together with porous microstructure obtained in the SEM characterization, it can be concluded that the measured results are consistent with the observations done on micrographs. Although grains were coarsened to 1.44-1.45 μm as a result of non-efficient packing at 0.40 solids content, no remarkable increase in grain sizes with increasing NaCl concentration was obtained. Apart from all the discussion above, when the results are examined, one of the most important points for this study stands out. Due to the phase transformation during the sintering, which was aforementioned in the literature review section, fully dense structure after sintering could not be achieved in any parameters as expected. It clearly shows the importance of particle packing and it can be concluded that even higher initial particle packing densities or further studies on sintering process are required. As already mentioned above, effect of seeding the thermodynamically stable phase into the green bodies will be discussed for further improvement in the sintered density results.

4.3. Effect of Seeding on Sintering Behaviour

Results of sintering after seeding the green bodies with stable phase can be seen on Fig.4.10. To reveal the effect of seeding on the achieving fully dense structure, solids content of 0.20 at 0.01 M NaCl concentration was chosen as benchmark parameter since this parameter gave the most promising result (95.7%) even without the seeding. After addition of seed, sintered density could be successfully improved up to almost 99%. Depending on the results, it can be concluded that amount of seeding does not really make difference on the sintered densities.

Even though there seems to be no important effect of changing the amount of seed powder on the sintered densities, increasing variation in the error margin with increasing seed amount was remarkable. Besides, increase in the variation of the sintered density results can be considered as unexpected results since the seed powder was commercially labeled as de-agglomerated. Yet, the SEM micrographs of the powder given in the Fig.3.1 made it clear that it was not the case and agglomerated, non-spherical morphology of the seed powder was obviously revealed. Therefore, this variation can be related with the increasing amount of agglomerated powder in the green body. This increase in agglomeration amount in the structure destructed the homogeneity and it led to an increase in the variability of the sintered results although there was no such a huge difference in the agglomerated powder amount between 3 and 5 wt.% seeding.

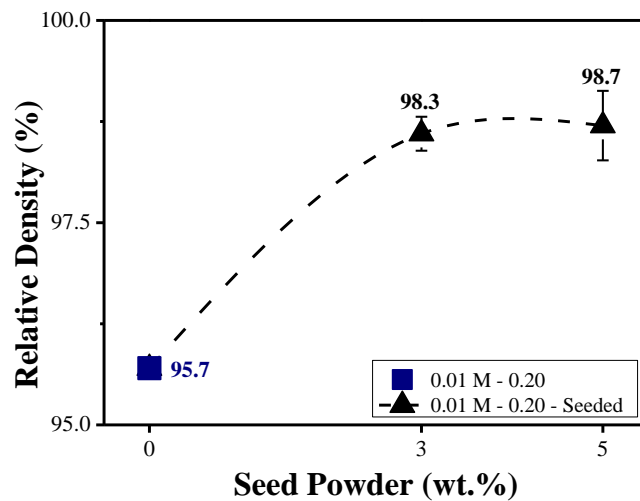


Figure 4.10. Effect of seeding and its amount on the sintered density at 0.20 solids content

In connection with this, effect of seeding and its agglomerated structure on the microstructure and average grain sizes can be seen on Fig.4.11 and Table 4.7. In addition to the effect of solids content on grain boundary evolution, grain coarsening was also obtained after seed addition. Increasing in irregularity in the shape of grains with higher amounts of seed powders should also be noted. However, these results can be considered as expected due to the agglomerated structure of seed powder.

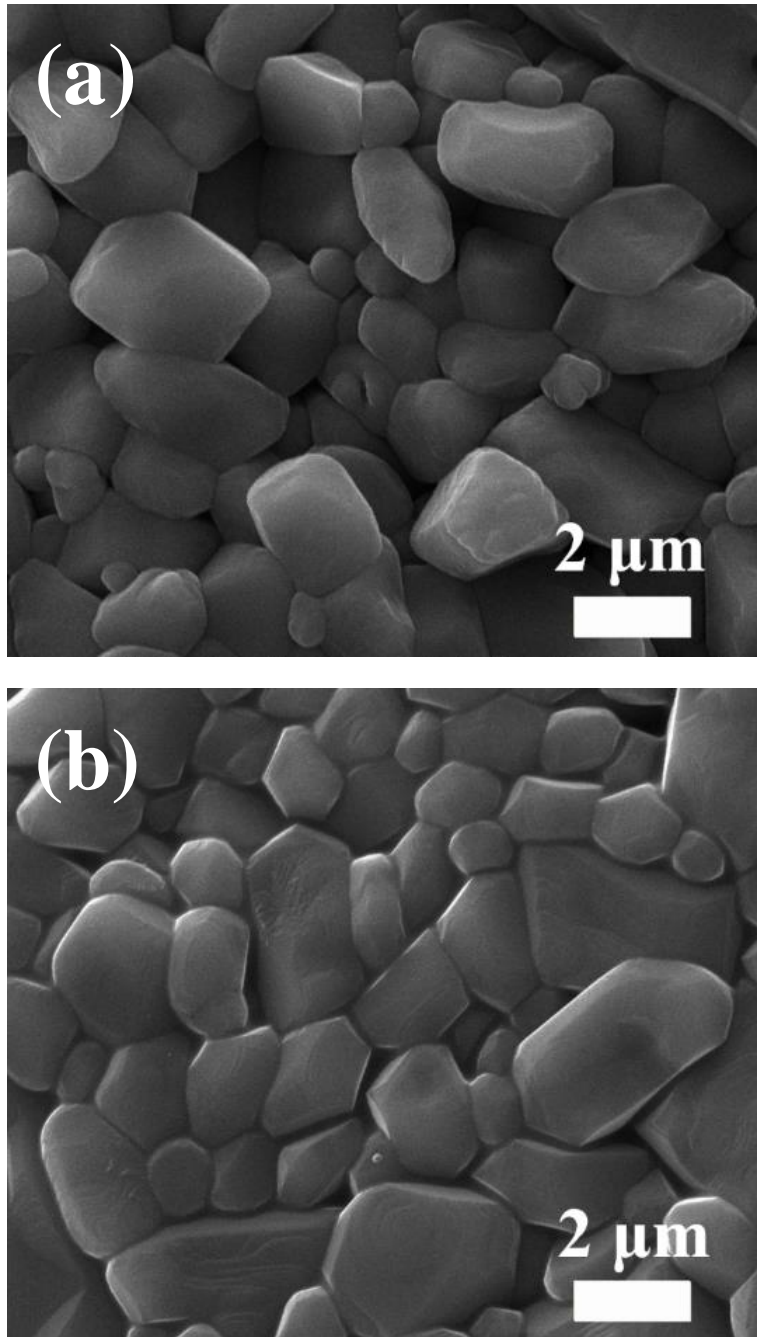


Figure 4.11. Effect of seeding and its amount on the microstructure of sintered bodies at 0.20 solids content. Seed amounts are (a) 3 wt.% (b) 5 wt.% of alumina powder

Table 4.7. *Effect of seed amount on grain size.*

Parameters [Amount of Seed (wt.%)]	<i>Intercept Length</i> (μm)
0	1.28
3	2.10
5	2.20

In addition, increased coarsening was observed in some of the grains with increasing amount of seed powder, while some remained small and medium-sized grains began to disappear. The increasing seed amount, addition of seeds as a sintering aid could increase the final density by few percent, but in expense to the irregular grain growth.

CHAPTER 5

EFFECT OF ASCORBIC ACID ON PARTICLE PACKING AND SINTERING BEHAVIOURS

5.1. Particle Packing Behaviour

In order to reveal the effect of ascorbic acid addition on the packing behavior of alumina nanopowder during slip casting, rheological behaviour of alumina suspensions with and without addition of ascorbic acid for various solids loading were first examined. (Fig. 5.1)

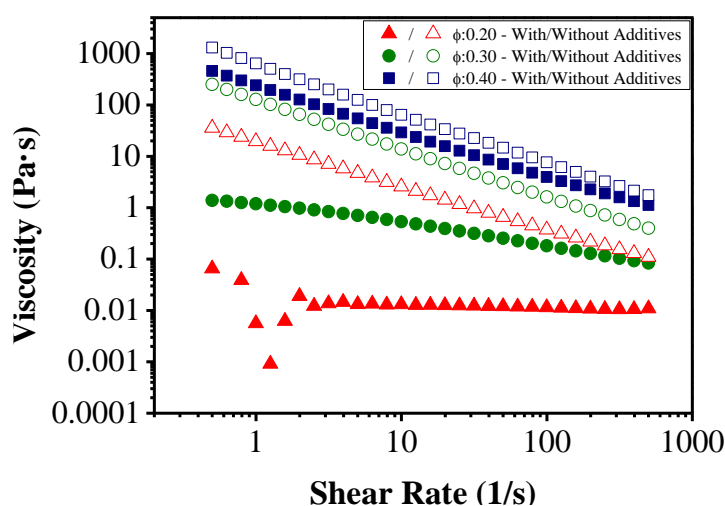


Figure 5.1. Effect of 1 wt.% ascorbic acid addition on the viscosity of nano-alumina suspensions with various solids content.

Due to the logarithmic relation between viscosity and the shear rate, the rheological behavior of suspensions were fit into power law relation (Eq.4.1) and the results were presented in Table 5.1.

Table 5.1. The power law parameters obtained from the rheological behavior of alumina nanopowder suspensions. As an additive 1 wt% ascorbic acid was used.

Φ	<i>no additive</i>		<i>with additives</i>		<i>The change in K with additives</i>
	<i>K</i>	<i>n</i>	<i>K</i>	<i>n</i>	
0.20	13.787	0.219	0.0151	0.941	- 89.1%
0.30	97.079	0.113	1.6822	0.516	-73.3%
0.40	549.19	0.073	163.4	0.196	-28.8%

Power Law: $\eta = K \cdot \dot{\gamma}^{n-1}$, where η is the suspension viscosity, K is the consistency coefficient and n is the power law index. R^2 for fitting of the rheological behavior of suspension with solids content of 0.20 with additives is 0.85, for others the value is larger than 0.999.

The consistency index (K) in power law is the indicator of the level of the viscosity over the range of applied shear rate. As realized in Table 5.1, the viscosity of suspensions reduced with addition of ascorbic acid regardless from the solids content of suspension. Yet, the effect of ascorbic acid addition was diminished as the solids content increased. While the consistency index could be reduced by 89% for solids loading of 0.20, the reduction on this value was about 73% and 29% for solids loading of 0.30 and 0.40, respectively. Considering very high initial viscosities, such a reduction was enough to obtain significant fluidity.

The power law index (n) shows the level of shear thinning behavior of suspensions such that the values close to 0 indicates a very shear thinning behavior while the values approaches to 1 indicates a Newtonian flow behavior. As shown in Table 5.1, addition of 1 wt% ascorbic acid to suspensions with solids content of 0.20 led to significant change in flow behavior from strong shear thinning character (n:0.219) to almost shear rate independent Newtonian flow (n:0.941) indicating that that the effect of attractive interparticle interactions were minimized. For higher solids content, the power law index increased and severe shear thinning behavior was observed. Regardless from the solids loading, the power law index decreased with addition of ascorbic acid indicating relatively more homogeneously dispersed stabilized suspensions.

In order to investigate the effect of ascorbic acid addition for alumina suspensions with various solids content, the suspensions were slip casted and the relative densities were measured (Figure 5.2). With increasing solids content, denser green bodies could be obtained. The increase in green density with solids loading of 0.40, the relative green density could be increased to 58%, which is one of the highest values reported in literature, particularly as a result of such a straightforward process.

The green densities of slip casted bodies increased almost linearly with increasing solids content from 51.1% to 53.5% and 58.0% when the solids content was increased from 0.20 to 0.30 and 0.40, respectively. However, no further increase in the green density could be achieved due to the extremely sharp increases in the viscosity when solids content was further increased probably because of the inavailability of interparticle spacing.

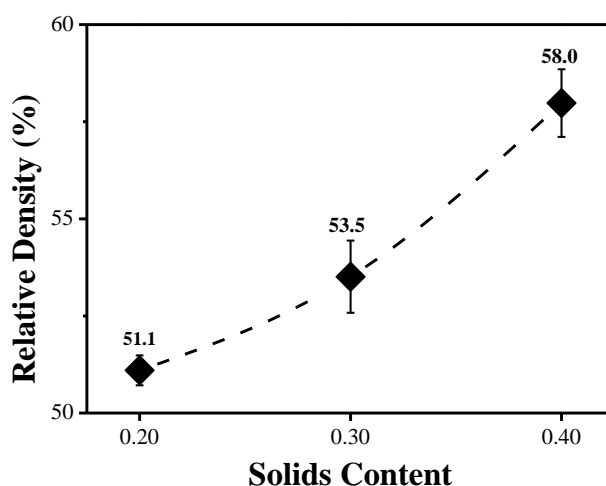


Figure 5.2. Particle packing densities with respect to solids content at 1 wt.% ascorbic acid concentration.

Even though these results were highly promising for applications requiring nanopowder suspensions with high solids contents, widening in error margin from 0.39% to 0.90% with higher solids contents should also be noted. It could be attributed to the increased density in agglomerated sites with higher solids content. In order to examine the particle packing behaviour of these slip-cast bodies, macro-micro and nano structures of the green bodies are given in the Fig.5.3.

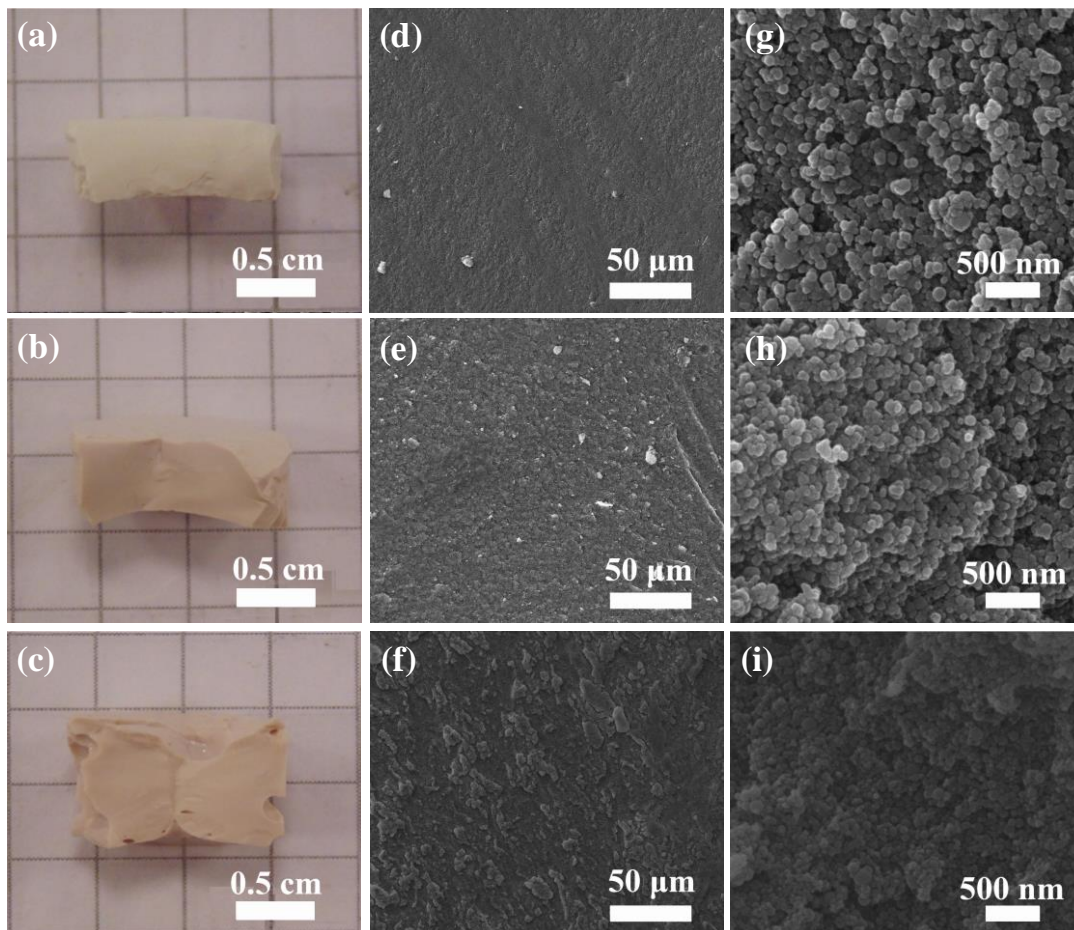


Figure 5.3. (a-c) Macro, (d-f) micro, (g-i) nano structures of bodies having 0.20, 0.30, 0.40 solids content from top to bottom respectively.

*(All suspensions constantly have 1 wt.% ascorbic acid concentration.)

As in shown in Fig. 5.3 (a-c), loss in smoothness with increasing solids contents can be realized with naked eye. Yet, the obtained surfaces were sufficiently poreless and they had relatively higher smoothness compared to the bodies in Chapter 4. Although the loss in smoothness was observed at higher solids content, observed smoothness and almost poreless structures, for such a high solids content like 0.40, were noteworthy compared to its fructose and NaCl added counterparts. These observations (Fig.5.2) were clearly consistent with the results obtained in the green densities (Fig.5.3). Like the naked eye observations done on the green bodies, similar loss in the smoothness on the surface was also observed on the microstructure of the bodies

(Fig.5.3 (d-f)). Relatedly, increase in the agglomerated sites with increasing solids content were obtained and, in relation to this, homogeneous uniform nano structure obtained in the 0.20 solids content has been replaced with relatively firm and agglomerated structure increasing with higher solids contents (Fig.5.3 (g-i)). Even though increase in agglomerated site density was observed, no porosity was observed in the packing structure (Fig.5.3 (f)). It was promising observation for such a highly loaded suspensions. Agglomerations, which started to increase at higher solids content, could be attributed to the new incoming particles disturbing the searching ability of particles to find low energy position and allowing less time for particle rearrangement due to the higher attractive interaction arising from reducing interparticle spacing. Michálková et al. [137] reported their study results showing that strong agglomerations, starting to appear with increasing solids contents, were settled into pore cavities, which, then, resulted in further increase in green density. Even though it decreased the maximum reachable final density, it was noted that it resulted in higher final densities compared to its porous counterparts. However, it resulted in lower final densities than the sintered densities of its counterparts having homogeneous particle packing structure even though its green densities were higher. Similarly, Tallon et al. [34] reported that sintered densities of alumina bodies, which had similar green densities but produced from suspensions having different viscosities, resulted in different results. According to this study, high viscosity samples resulted in lower sintered densities while their low viscosity counterparts resulted in higher densities. From this point of view, the results to be obtained from micrographs of particle packing and results of sintering density would be more descriptive.

5.2. Sintering Behaviour

Green bodies were sintered at 1600 °C for 2 hours in order to achieve fully dense structure. Overall, all of the samples achieved sintered density results around 90% of the theoretical density. When the micrographs of particle packing of both of the studies were investigated (Fig.4.3 and Fig.5.3), these results could be related with that fructose

and NaCl added bodies had severe increasing in agglomerated sites with interconnected pore structures at higher solids content while ascorbic acid added bodies had slightly increasing agglomerated sites in the structure (relatively more homogeneous packing) with higher solids content. Besides, ascorbic acid added bodies had the advantage of starting from high green densities. At the end, bodies could be easily sintered to densities around 90% in shorter times and pore-generating agglomeration was not operative too much.

Apart from these, the lowest sintered density in ascorbic acid study obtained at solids content of 0.30. Despite the fact that it did not have the lowest green density. This observation could be attributed to the increase in the agglomeration in the particle packing structure while the green density could only be increased slightly. In summary, advantage acquired from higher green density could not be utilized in this solids content since the agglomeration produced new pores during sintering. However, remarkable increase in green density at 0.40 solids content and poreless structure compensated the agglomerations in packing structure. Yet, it should be noted that the sintered densities were not significantly different over the solids content studied ($91\% \pm 2$) to conclude that there was a meaningful and significant difference and all these values were significantly high when compared to the studies in the literature. Sintered density of bodies at 0.40 solids content was one of the highest final density achieved with such a straightforward process and conventional sintering without aids.

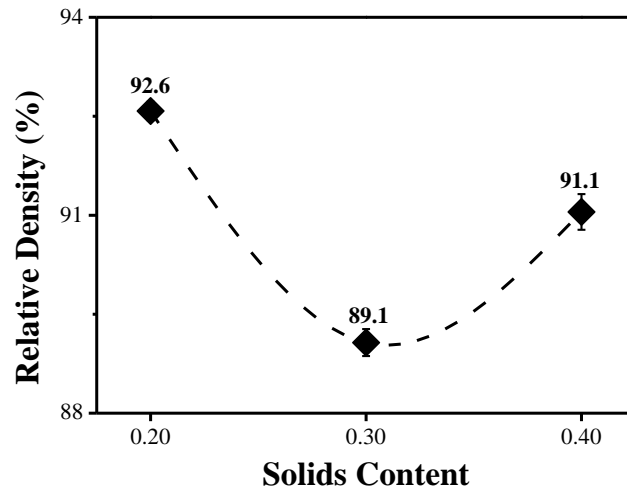


Figure 5.4. Effect of solids content on the sintered densities at 1 wt.% ascorbic acid concentration.

Table 5.2. Effect of solids content on average grain sizes

Parameters [Solids content]	Intercept Length (μm)
0.20	0.82
0.30	0.85
0.40	0.91

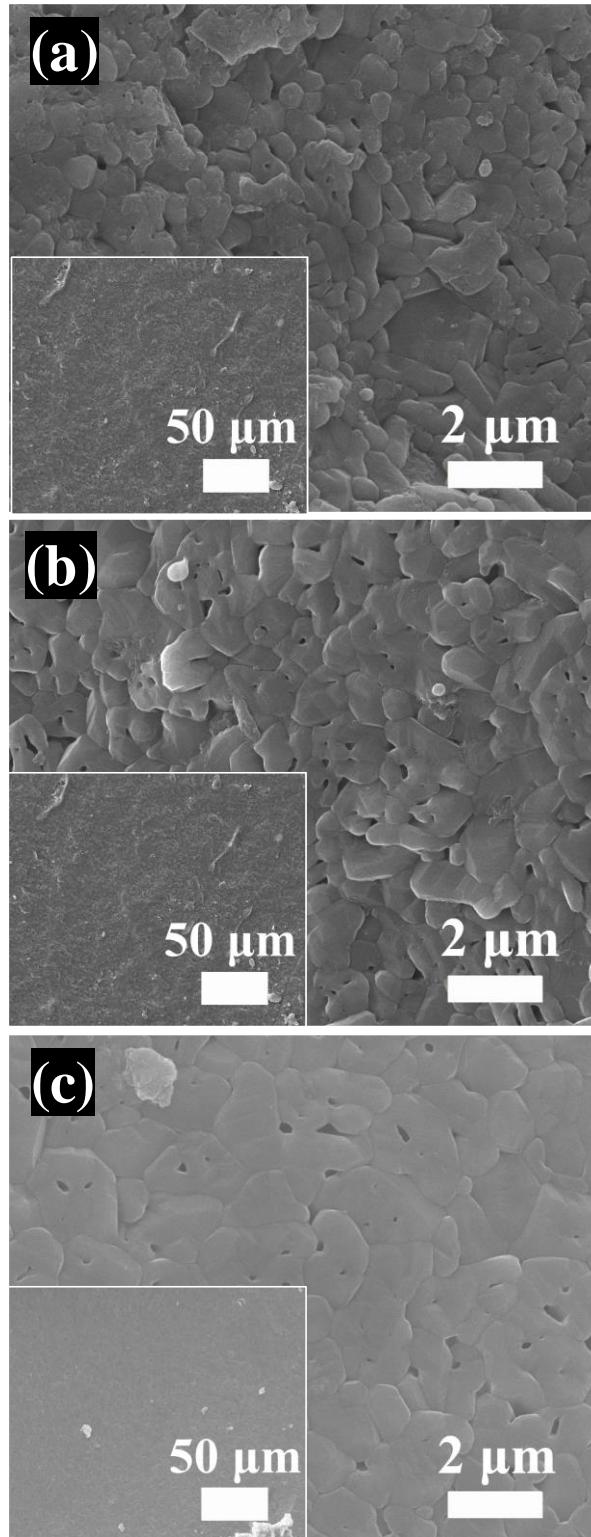


Figure 5.5. Microstructures of sintered bodies having (a) 0.20, (b) 0.30, (c) 0.40 solids content respectively

As expected from similarity of the sintered densities, microstructures of the sintered bodies were similar and almost poreless. However, the grain sizes were measured different. It was obtained that average grain size slightly increased with higher solids contents from 0.82 μm to 0.85 μm and 0.91 μm when the solids content was increased from 0.20 to 0.30 and 0.40, respectively. As it was reported in the literature that the agglomerated structure and disrupted homogeneity of particle packing led to grain coarsening, it could be concluded from the widening in the error margin and the grain coarsening with increasing solids content that agglomeration and inhomogeneity in the particle packing structure is the reason of these results. Yet, relatively more homogeneous and poreless structure of ascorbic acid added bodies, compared to fructose and NaCl added bodies, resulted in sub-micron sized grain boundaries.

Overall, it can be concluded that with addition of 1 wt.% ascorbic acid, alumina nanopowders were homogeneously dispersed and closely packed, leading to high density end product without using any complex process.

5.3. Effect of Seeding on Sintering Behaviour

In order to further increase the final density, effect of sintering aid, $\alpha\text{-Al}_2\text{O}_3$ seeds, on final density was studied. In order to obtain the higher end product density, the suspensions with solids loading of 0.20 was used. Fig.5.6 shows the effect of sub-micron sized $\alpha\text{-Al}_2\text{O}_3$ seed addition. As seen in this figure, with addition of seed, the green densities could be increased to 98% and 99% with addition of 3 wt.% and 5 wt.%

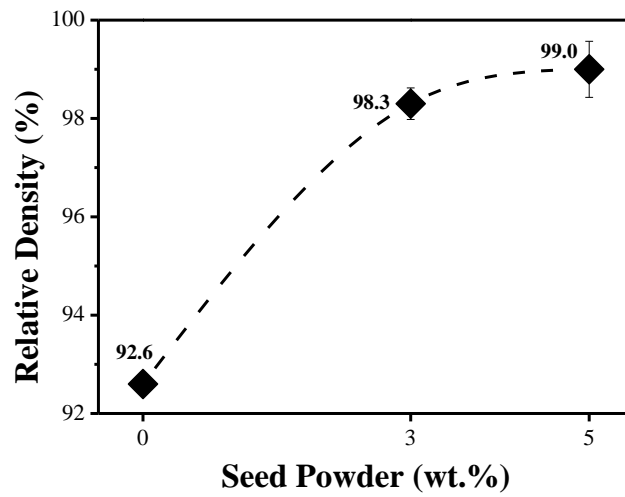


Figure 5.6. Effect of seeding and its amount on sintered densities.

In consistency with the results discussed and given before, grain coarsening was obtained even in micrographs since the agglomeration and non-homogeneous packing may cause grain coarsening with increasing seed amounts.

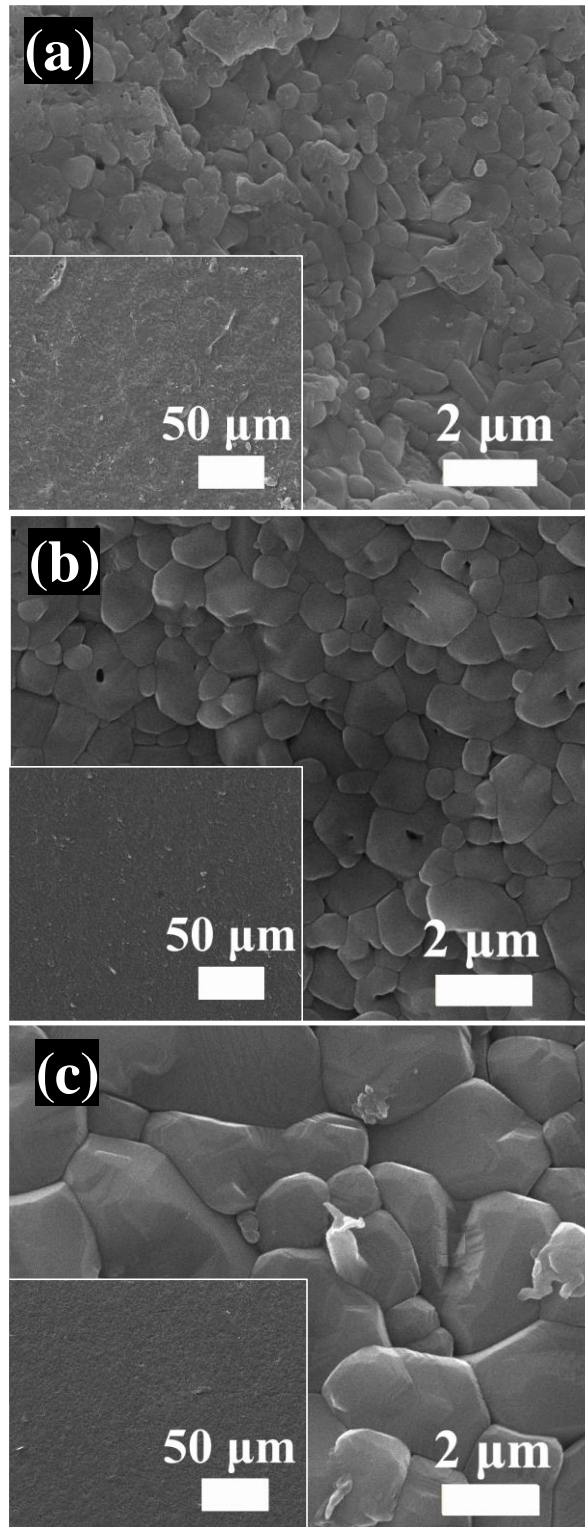


Figure 5.7. Effect of seeding and its amount on the microstructure of seeding samples having solids content of 0.20. (a) 0 wt.%, (b) 3 wt.%, (c) 5 wt.% of seed powders.

Table 5.3. *Effect of seed amount on grain size of sintered bodies constantly at 0.20 solids content*

Parameters [Amount of Seed (wt.)]	<i>Intercept Length</i> (μm)
0	0.82
3	1.61
5	2.60

Microstructures of the sintered bodies after sintering and average grain sizes is given in the Fig.5.7. and Table 5.3. Significant grain coarsening with addition of seed, as expected. The grain size was increased from 0.82 μm to 1.61 μm at seed amount of 3 wt.% and it was increased more than 3-fold at 5 wt.% (2.60 μm). Similarly, with combined effect (Fig.4.12), observation of increasing in irregularity of the shape of grains should also be noted.

CHAPTER 6

CONCLUSIONS

Production of pore-free, high density advanced ceramics from nanopowders is a challenge because of the unexpectedly high viscosities of their suspensions and resulting inhomogeneous and loose packing of powders. This thesis aimed to unveil the relation between the rheological behavior and packing structure of nanopowders in order to obtain high density advanced ceramics via conventional techniques. As a result of literature review, two of the most effective dispersants were chosen and their effects on the rheological behavior of suspensions, particle packing, and densities of green and sintered bodies were studied.

In the first approach, fructose and NaCl were used as additives in order to control hydration and electric double layers formed around alumina nanopowders. It was revealed that the interparticle spacing between nanopowders were significantly small compared to the sub-micron size powder suspensions, and the additions of fructose and NaCl could effectively adjust the hydration and electric double layer thickness, respectively, and free up more space for particle movement. The Fank and Dinger's model for IPS calculations were modified for aqueous suspensions of nanopowders (IPSAq), and the resulting model could successfully explain the rheological and particle packing behavior for nanopowder suspensions.

As a result of IPSaq optimization with fructose and NaCl additions, the relative green body density as high as 52.7% was obtained when suspensions with solids content of 0.20 was used. Efficient packing of particles with homogeneous dispersions in green body could be obtained. As a result, the relative sintered densities as high as 92.7% could be achieved. The average grain size was about 1.3 μm . These densities are one of the highest end-product density obtained for nanopowder systems reported in open

literature, and are particularly interesting as they are obtained through a straightforward process and conventional sintering without using any sintering aids.

In order to further increase the final densities, α -Al₂O₃ was used as a sintering aid for the samples prepared from suspensions with solids loading of 0.20. By this way, the relative sintered density increased to 99%, but the average grain size also increased to 2.2 μ m.

When solids content increased to 0.40, the green density decreased to 46.5% and large interconnected pores were observed. Enlarging the IPSaq with shrinkage of electric double layer, the green density could be increased to 52.3% and large pores can be eliminated. However, when sintered, the relative density of 76.2% was obtained. The lower value of the sintered density explained with the high number of agglomeration sites placed in large pores. As a result of inhomogeneous packing, the average grain size increased to 1.5 μ m. The results showed that the high green density does not always lead to high sintered densities.

In the second approach, ascorbic acid was used as an additive. Ascorbic acid addition reduced the viscosity of suspensions with solids loading between 0.20 and 0.40. The relative green densities of slip cast bodies obtained from these suspensions almost linearly increased with increasing solids content, and reached to 58% at solids loading of 0.40. Homogeneously distributed particles was observed in green body structure. When sintered, the relative densities as high as 90% were observed for all solids content unlike the first approach. The grains in sintered bodies were below 1 μ m (about 0.8 μ m) for all structures, indicating that the use of ascorbic acid led to better dispersed suspensions and resulted in more closely packed green bodies when compared to the first approach.

α -Al₂O₃ seed addition into the suspensions with solids loading of 0.20 and 1 wt% ascorbic acid addition resulted in final density of 99%. Yet, excessive grain coarsening also observed in the second approach and average grain size of 2.6 μ m is reported.

For applications requiring high solids content, such as robocasting, use of ascorbic acid can be suggested. Such an application is expected to be one of the first examples in open literature where a highly loaded feedstock is prepared solely from nanopowders.

REFERENCES

- [1] M.N. Rahaman, *Ceramic processing and sintering*, M. Dekker, 2003.
- [2] G. V. Franks, C. Tallon, A.R. Studart, M.L. Sesso, S. Leo, Colloidal processing: enabling complex shaped ceramics with unique multiscale structures, *J. Am. Ceram. Soc.* 100 (2017) 458–490.
- [3] C. Herring, Effect of change of scale on sintering phenomena, *J. Appl. Phys.* 21 (1950) 301–303.
- [4] H. Song, R.L. Coble, R.J. Brook, Applicability of Herring’s scaling law to the sintering of powders., in: *Mater. Sci. Res.*, Plenum Press, 1984: pp. 63–79.
- [5] S. Jailani, G. V. Franks, T.W. Healy, ζ Potential of Nanoparticle Suspensions: Effect of Electrolyte Concentration, Particle Size, and Volume Fraction, *J. Am. Ceram. Soc.* 91 (2008) 1141–1147.
- [6] J.J. Gulicovski, L.S. Čerović, S.K. Milonjić, Point of Zero Charge and Isoelectric Point of Alumina, *Mater. Manuf. Process.* 23 (2008) 615–619.
- [7] B. Rand, R. Fries, Viscoelasticity of nano-alumina dispersions, *Ceram. Trans.* 62 (1996) 165–172.
- [8] M. Schneider, J. Claverie, C. Graillat, T.F. McKenna, High solids content emulsions. I. A study of the influence of the particle size distribution and polymer concentration on viscosity, *J. Appl. Polym. Sci.* 84 (2002) 1878–1896.
- [9] Intermolecular Force, *Interface Sci. Technol.* 18 (2011) 1–57.
- [10] J.H. Adair, E. Suvaci, J. Sindel, *Surface and Colloid Chemistry*, *Encycl. Mater. Sci. Technol.* (2001) 1–10.
- [11] B. V. Derjaguin, N. V. Churaev, V.M. Muller, *The Derjaguin—Landau—Verwey—Overbeek (DLVO) Theory of Stability of Lyophobic Colloids*, in: *Surf. Forces*, Springer US, Boston, MA, 1987: pp. 293–310.
- [12] Derjaguin, B. and Landau, L.D. (1941) Theory of the Stability of Strongly Charged Lyophobic Sols and of the Adhesion of Strongly Charged Particles in Solutions of Electrolytes. *Acta Physicochimica U.R.S.S.*, 14, 633-662.
- [13] Verwey, E.J.W. and Overbeek, J.Th.G. (1948) *Theory of the Stability of Lyophobic Colloids The Interaction of Sol Particles Having an Electric Double Layer*. Elsevier, Amsterdam.
- [14] J.N. Israelachvili, *Intermolecular and surface forces*, Academic Press, 2011.
- [15] M.N. Rahaman, *Theory of Solid-State and Viscous Sintering*, in: *Ceram.*

- Process. Sintering, Second Ed., M. Dekker, 2003: pp. 470–539.
- [16] E. Piacenza, A. Presentato, R.J. Turner, Stability of biogenic metal(loid) nanomaterials related to the colloidal stabilization theory of chemical nanostructures, *Crit. Rev. Biotechnol.* 38 (2018) 1137–1156.
 - [17] J.E. Funk, D.R. Dinger, Slip Control Using Particle-Size Analysis and Specific Surface Area | James E. Funk, *Am. Ceram. Soc. Bull.* 67 (1988) 890–894.
 - [18] T. Hao, R.E. Riman, Calculation of interparticle spacing in colloidal systems, *J. Colloid Interface Sci.* 297 (2006) 374–377.
 - [19] J.C. Berg, *An introduction to interfaces & colloids: the bridge to nanoscience*, World Scientific, 2010.
 - [20] R.G. Larson, *The structure and rheology of complex fluids*, Oxford University Press, 1999.
 - [21] V. VAND, Theory of Viscosity of Concentrated Suspensions, *Nature.* 155 (1945) 364–365.
 - [22] I.M. Krieger, T.J. Dougherty, A Mechanism for Non-Newtonian Flow in Suspensions of Rigid Spheres, *Trans. Soc. Rheol.* 3 (1959) 137–152.
 - [23] V. Starov, V. Zhdanov, M. Meireles, C. Molle, Viscosity of concentrated suspensions: influence of cluster formation, *Adv. Colloid Interface Sci.* 96 (2002) 279–293.
 - [24] D.-M. Liu, Particle packing and rheological property of highly-concentrated ceramic suspensions: ϕ_m determination and viscosity prediction, *J. Mater. Sci.* 35 (2000) 5503–5507.
 - [25] B.A. Horri, P. Ranganathan, C. Selomulya, H. Wang, A new empirical viscosity model for ceramic suspensions, *Chem. Eng. Sci.* 66 (2011) 2798–2806.
 - [26] † and Emilio Ruiz-Reina*, F. Carrique‡, Electroviscous Effect of Concentrated Colloidal Suspensions in Salt-Free Solutions, (2006).
 - [27] A. Ogawa, H. Yamada, S. Matsuda, K. Okajima, M. Doi, Viscosity equation for concentrated suspensions of charged colloidal particles, *J. Rheol. (N. Y. N. Y.)* 41 (1997) 769–785.
 - [28] P. Singh, K. Anoop, H. Patel, T. Sundararajan, T. Pradeep, S. Das, Anomalous Size Dependent Rheological Behavior of Alumina Based Nanofluids, *Int. J. Micro-Nano Scale Transp.* 1 (2010) 179–188.
 - [29] A. Ghadimi, R. Saidur, H.S.C. Metselaar, A review of nanofluid stability properties and characterization in stationary conditions, *Int. J. Heat Mass Transf.* 54 (2011) 4051–4068.

- [30] I.M. Mahbubul, R. Saidur, M.A. Amalina, Latest developments on the viscosity of nanofluids, *Int. J. Heat Mass Transf.* 55 (2012) 874–885.
- [31] Y. Rao, Nanofluids: Stability, phase diagram, rheology and applications, *Particuology*. 8 (2010) 549–555.
- [32] T. Wang, X. Wang, Z. Luo, M. Ni, K. Cen, Mechanisms of Viscosity Increase for Nanocolloidal Dispersions, *J. Nanosci. Nanotechnol.* 11 (2011) 3141–3150.
- [33] E. Forbes, D.J. Bradshaw, G. V. Franks, Temperature sensitive polymers as efficient and selective flotation collectors, *Miner. Eng.* 24 (2011) 772–777.
- [34] C. Tallon, M. Limacher, G. V. Franks, Effect of particle size on the shaping of ceramics by slip casting, *J. Eur. Ceram. Soc.* 30 (2010) 2819–2826.
- [35] M. Azar, P. Palmero, M. Lombardi, V. Garnier, L. Montanaro, G. Fantozzi, J. Chevalier, Effect of initial particle packing on the sintering of nanostructured transition alumina, *J. Eur. Ceram. Soc.* 28 (2008) 1121–1128.
- [36] G. Tari, J.M.F. Ferreira, A.T. Fonseca, O. Lyckfeldt, Influence of particle size distribution on colloidal processing of alumina, *J. Eur. Ceram. Soc.* 18 (1998) 249–253.
- [37] J.C. Kim, K.H. Auh, C.H. Schilling, Effects of polysaccharides on the particle packing and green strength of alumina slurries, *Mater. Lett.* 40 (1999) 209–212.
- [38] J. Ma, L.C. Lim, Effect of particle size distribution on sintering of agglomerate-free submicron alumina powder compacts, *J. Eur. Ceram. Soc.* 22 (2002) 2197–2208.
- [39] M. Aminzare, M. Mazaheri, F. Golestani-fard, H.R. Rezaie, R. Ajeian, Sintering behavior of nano alumina powder shaped by pressure filtration, *Ceram. Int.* 37 (2011) 9–14.
- [40] W. Liu, Z. Xie, Pressureless Sintering Behavior of Injection Molded Alumina Ceramics, *Sci. Sinter.* 46 (2014) 3–13.
- [41] A.R. Olszyna, P. Marchlewski, K.J. Kurzydłowski, Sintering of high-density, high-purity alumina ceramics, *Ceram. Int.* 23 (1997) 323–328.
- [42] K. Lu, Theoretical analysis of colloidal interaction energy in nanoparticle suspensions, *Ceram. Int.* 34 (2008) 1353–1360.
- [43] M. Iijima, H. Kamiya, Surface Modification for Improving the Stability of Nanoparticles in Liquid Media, *KONA Powder Part. J.* 27 (2009) 119–129.
- [44] S. Çınar, M. Akinc, Electrostatic Stabilization of Alumina Nanopowder Suspensions, *Sci. Adv. Mater.* 6 (2014) 520–529.
- [45] H. Meryman, Review of biological freezing. In “Cryobiology”. Ed.: HT

- Meryman, (1966).
- [46] S.E. Charm, P. Moody, Bound water in haddock muscle, *Ashrae J.* (1966) 39–42.
 - [47] J.H. Moy, K.-C. Chan, A.M. Dollar, Bound water in fruit products by the freezing method, *J. Food Sci.* 36 (1971) 498–499.
 - [48] C. Li, M. Akinc, J. Wiench, M. Pruski, C.H. Schilling, Relationship Between Water Mobility and Viscosity of Nanometric Alumina Suspensions, *J. Am. Ceram. Soc.* 88 (2005) 2762–2768.
 - [49] S. Çınar, L. van Steenhuyse, M. Akinc, Elucidation of Viscosity Reduction Mechanism of Nano Alumina Suspensions with Fructose Addition by DSC, *J. Am. Ceram. Soc.* 96 (2013) 1077–1084.
 - [50] C. Li, M. Akinc, Role of Bound Water on the Viscosity of Nanometric Alumina Suspensions, *J. Am. Ceram. Soc.* 88 (2005) 1448–1454.
 - [51] N. Katsiris, A. Kouzeli-Katsiri, Bound water content of biological sludges in relation to filtration and dewatering, *Water Res.* 21 (1987) 1319–1327.
 - [52] C.H. Schilling, M. Sikora, P. Tomasik, C. Li, V. Garcia, Rheology of alumina–nanoparticle suspensions: effects of lower saccharides and sugar alcohols, *J. Eur. Ceram. Soc.* 22 (2002) 917–921.
 - [53] P. Falkowski, P. Bednarek, A. Danelska, T. Mizerski, M. Szafran, Application of monosaccharides derivatives in colloidal processing of aluminum oxide, *J. Eur. Ceram. Soc.* 30 (2010) 2805–2811.
 - [54] E. Firlar, S. Çınar, S. Kashyap, M. Akinc, T. Prozorov, Direct Visualization of the Hydration Layer on Alumina Nanoparticles with the Fluid Cell STEM in situ, *Sci. Rep.* 5 (2015) 9830.
 - [55] S. Cinar, Rheological behavior of oxide nanopowder suspensions, Iowa State University, Digital Repository, 2013.
 - [56] S. Çınar, D.D. Anderson, M. Akinc, Combined effect of fructose and NaCl on the viscosity of alumina nanopowder suspensions, *J. Eur. Ceram. Soc.* 35 (2015) 377–382.
 - [57] J.A. Lewis, Colloidal Processing of Ceramics, *J. Am. Ceram. Soc.* (2004).
 - [58] P.S. Bhosale, J.C. Berg, Poly(acrylic acid) as a rheology modifier for dense alumina dispersions in high ionic strength environments, *Colloids Surfaces A Physicochem. Eng. Asp.* 362 (2010) 71–76.
 - [59] P. Bowen, C. Carry, D. Luxembourg, H. Hofmann, Colloidal processing and sintering of nanosized transition aluminas, *Powder Technol.* 157 (2005) 100–107.

- [60] O. Lyckfeldt, L. Palmqvist, E. Carlström, Stabilization of alumina with polyelectrolyte and comb copolymer in solvent mixtures of water and alcohols, *J. Eur. Ceram. Soc.* 29 (2009) 1069–1076.
- [61] C.H. Schilling, M. Sikora, P. Tomasik, C. Li, V. Garcia, Rheology of alumina–nanoparticle suspensions: effects of lower saccharides and sugar alcohols, *J. Eur. Ceram. Soc.* 22 (2002) 917–921.
- [62] P. Tomasik, C.H. Schilling, R. Jankowiak, J.-C. Kim, The role of organic dispersants in aqueous alumina suspensions, *J. Eur. Ceram. Soc.* 23 (2003) 913–919.
- [63] S. Çınar, M. Akinc, Ascorbic acid as a dispersant for concentrated alumina nanopowder suspensions, *J. Eur. Ceram. Soc.* 34 (2014) 1997–2004.
- [64] Dispersant Technology for Red and Yellow Iron Oxides | 2016-06-01 | PCI Magazine, (n.d.).
- [65] J. CESARANO, I.A. AKSAY, Processing of Highly Concentrated Aqueous alpha-Alumina Suspensions Stabilized with Polyelectrolytes, *J. Am. Ceram. Soc.* 71 (1988) 1062–1067.
- [66] B.J. Briscoe, A.U. Khan, P.F. Luckham, Optimising the dispersion on an alumina suspension using commercial polyvalent electrolyte dispersants, *J. Eur. Ceram. Soc.* 18 (1998) 2141–2147.
- [67] B.P. Singh, S. Bhattacharjee, L. Besra, D.K. Sengupta, Evaluation of dispersibility of aqueous alumina suspension in presence of Darvan C, *Ceram. Int.* 30 (2004) 939–946.
- [68] B.P. Singh, S. Bhattacharjee, L. Besra, D.K. Sengupta, Electrokinetic and adsorption studies of alumina suspensions using Darvan C as dispersant, *J. Colloid Interface Sci.* 289 (2005) 592–596.
- [69] S.W. Sofie, F. Dogan, Freeze Casting of Aqueous Alumina Slurries with Glycerol, *J. Am. Ceram. Soc.* 84 (2004) 1459–1464.
- [70] A. Tsetsekou, C. Agrafiotis, A. Miliadis, Optimization of the rheological properties of alumina slurries for ceramic processing applications Part I: Slip-casting, *J. Eur. Ceram. Soc.* 21 (2001) 363–373.
- [71] J.F. Kelso, T.A. Ferrazzoli, Effect of Powder Surface Chemistry on the Stability of Concentrated Aqueous Dispersions of Alumina, *J. Am. Ceram. Soc.* 72 (1989) 625–627.
- [72] H.-H. Tang, M.-L. Chiu, H.-C. Yen, Slurry-based selective laser sintering of polymer-coated ceramic powders to fabricate high strength alumina parts, *J. Eur. Ceram. Soc.* 31 (2011) 1383–1388.
- [73] L. Jiang, L. Gao, Effect of Tiron adsorption on the colloidal stability of nano-

- sized alumina suspension, *Mater. Chem. Phys.* 80 (2003) 157–161.
- [74] A.U. Khan, B.J. Briscoe, P.F. Luckham, Interaction of binders with dispersant stabilised alumina suspensions, *Colloids Surfaces A Physicochem. Eng. Asp.* 161 (2000) 243–257.
- [75] J.J. Gulicovski, L.S. Čerović, S.K. Milonjić, Stability of alumina suspensions in the presence of Tiron, *Ceram. Int.* 34 (2008) 23–26.
- [76] C.H. Schilling, R.A. Bellman, R.M. Smith, H. Goel, H. Giesche, Plasticizing Aqueous Suspensions of Concentrated Alumina with Maltodextrin Sugar, *J. Am. Ceram. Soc.* 82 (2004) 57–66.
- [77] M. Sikora, C.H. Schilling, P. Tomasik, C. Li, Dextrin plasticizers for aqueous colloidal processing of alumina, *J. Eur. Ceram. Soc.* 22 (2002) 625–628.
- [78] P. Tomasik, C.H. Schilling, R. Jankowiak, J.-C. Kim, The role of organic dispersants in aqueous alumina suspensions, *J. Eur. Ceram. Soc.* 23 (2003) 913–919.
- [79] B.M. Cerrutti, C.S. de Souza, A. Castellan, R. Ruggiero, E. Frollini, Carboxymethyl lignin as stabilizing agent in aqueous ceramic suspensions, *Ind. Crops Prod.* 36 (2012) 108–115.
- [80] M. Acosta, V.L. Wiesner, C.J. Martinez, R.W. Trice, J.P. Youngblood, Effect of Polyvinylpyrrolidone Additions on the Rheology of Aqueous, Highly Loaded Alumina Suspensions, *J. Am. Ceram. Soc.* 96 (2013) 1372–1382.
- [81] C. Xiao, H. Chen, X. Yu, L. Gao, L. Guo, Dispersion of Aqueous Alumina Suspensions with Biodegradable Polymers, *J. Am. Ceram. Soc.* 94 (2011) 3276–3281.
- [82] G. V. Franks, C. Tallon, A.R. Studart, M.L. Sesso, S. Leo, Colloidal processing: enabling complex shaped ceramics with unique multiscale structures, *J. Am. Ceram. Soc.* 100 (2017) 458–490.
- [83] S. Mamatha, P. Biswas, P. Ramavath, D. Das, R. Johnson, 3D printing of complex shaped alumina parts, *Ceram. Int.* (2018).
- [84] T. Schlordt, F. Keppner, N. Travitzky, P. Greil, Robocasting of Alumina Lattice Truss Structures, *J. Ceram. Sci. Tech.* (2012).
- [85] T. Schlordt, S. Schwanke, F. Keppner, T. Fey, N. Travitzky, P. Greil, Robocasting of alumina hollow filament lattice structures, *J. Eur. Ceram. Soc.* 33 (2013) 3243–3248.
- [86] J.E. Smay, J. Cesarano, J.A. Lewis, Colloidal inks for directed assembly of 3-D periodic structures, *Langmuir.* (2002).
- [87] J.A. Lewis, Direct ink writing of 3D functional materials, *Adv. Funct. Mater.*

- (2006).
- [88] J.N. Stuecker, J. Cesarano, D.A. Hirschfeld, Control of the viscous behavior of highly concentrated mullite suspensions for robocasting, *J. Mater. Process. Technol.* (2003).
- [89] C. Zhu, J.E. Smay, Thixotropic rheology of concentrated alumina colloidal gels for solid freeform fabrication, *J. Rheol.* (N. Y. N. Y). (2011).
- [90] T. Kakui, T. Miyauchi, H. Kamiya, Analysis of the action mechanism of polymer dispersant on dense ethanol alumina suspension using colloidal probe AFM, *J. Eur. Ceram. Soc.* 25 (2005) 655–661.
- [91] A.R. Studart, E. Amstad, M. Antoni, L.J. Gauckler, Rheology of Concentrated Suspensions Containing Weakly Attractive Alumina Nanoparticles, *J. Am. Ceram. Soc.* 89 (2006) 2418–2425.
- [92] A.R. Studart, E. Amstad, L.J. Gauckler, Colloidal Stabilization of Nanoparticles in Concentrated Suspensions, *Langmuir.* 23 (2007) 1081–1090.
- [93] A.. Studart, V.. Pandolfelli, E. Tervoort, L.. Gauckler, Selection of dispersants for high-alumina zero-cement refractory castables, *J. Eur. Ceram. Soc.* 23 (2003) 997–1004.
- [94] S. Desset-Brèthes, B. Cabane, O. Spalla, Competition Between Ligands for Al₂O₃ in Aqueous Solution, *J. Phys. Chem. A.* 116 (2012) 6511–6518.
- [95] P.C. Hidber, T.J. Graule, L.J. Gauckler, Citric Acid-A Dispersant for Aqueous Alumina Suspensions, *J. Am. Ceram. Soc.* 79 (1996) 1857–1867.
- [96] H. Husin, Y.-K. Leong, J. Liu, Molecular attributes of an effective steric agent: Yield stress of dispersions in the presence of pure enantiomeric and racemate malic acids, *Adv. Powder Technol.* 23 (2012) 459–464.
- [97] Y.-K. Leong, Role of Molecular Architecture of Citric and Related Polyacids on the Yield Stress of α -Alumina Slurries: Inter- and Intramolecular Forces, *J. Am. Ceram. Soc.* 93 (2010) 2598–2605.
- [98] J.C. Kim, C.H. Schilling, P. Tomasik, K.H. Auh, Plasticizing dense alumina slurries with mono- and di-saccharides, *Mater. Lett.* 42 (2000) 221–224.
- [99] Y. Yar, F.Y. Acar, E. Yurtsever, M. Akinc, Reduction of Viscosity of Alumina Nanopowder Aqueous Suspensions by the Addition of Polyalcohols and Saccharides, *J. Am. Ceram. Soc.* 93 (2010) 2630–2636.
- [100] A.. Studart, V.. Pandolfelli, E. Tervoort, L.. Gauckler, Selection of dispersants for high-alumina zero-cement refractory castables, *J. Eur. Ceram. Soc.* 23 (2003) 997–1004.
- [101] P. Wicinska, A. Wieclaw, F. Bilski, Selected sugar acids as highly effective

- deflocculants for concentrated nanoalumina suspensions, *J. Eur. Ceram. Soc.* 37 (2017) 4033–4041.
- [102] V. Prajzler, D. Salamon, K. Maca, Pressure-less rapid rate sintering of pre-sintered alumina and zirconia ceramics, *Ceram. Int.* 44 (2018) 10840–10846.
- [103] G. Maizza, S. Grasso, Y. Sakka, Systematic study on densification of alumina fine powder during milliwave sintering at 28 GHz, *J. Asian Ceram. Soc.* 2 (2014) 215–222.
- [104] P. Bowen, C. Carry, D. Luxembourg, H. Hofmann, Colloidal processing and sintering of nanosized transition aluminas, *Powder Technol.* 157 (2005) 100–107.
- [105] T.K. GUPTA, Possible Correlation Between Density and Grain Size During Sintering, *J. Am. Ceram. Soc.* 55 (1972) 276–277.
- [106] E. Levänen, T. Mäntylä, Effect of sintering temperature on functional properties of alumina membranes, *J. Eur. Ceram. Soc.* (2002).
- [107] S. Lartigue-Korinek, C. Legros, C. Carry, F. Herbst, Titanium effect on phase transformation and sintering behavior of transition alumina, *J. Eur. Ceram. Soc.* 26 (2006) 2219–2230.
- [108] C.S. Nordahl, G.L. Messing, Transformation and densification of nanocrystalline θ -alumina during sinter forging, *J. Am. Ceram. Soc.* (1996).
- [109] C.S. Nordahl, G.L. Messing, Sintering of α -Al₂O₃-seeded nanocrystalline γ -Al₂O₃ powders, *J. Eur. Ceram. Soc.* 22 (2002) 415–422.
- [110] C. Legros, C. Carry, P. Bowen, H. Hofmann, Sintering of a transition alumina: effects of phase transformation, powder characteristics and thermal cycle, *J. Eur. Ceram. Soc.* 19 (1999) 1967–1978.
- [111] S.J. Wu, L.C. Jonghe, M.N. Rahaman, Sintering of Nanophase gamma-Al₂O₃ Powder, *J. Am. Ceram. Soc.* 79 (1996) 2207–2211.
- [112] J. Zheng, J.S. Reed, Effects of Particle Packing Characteristics on Solid-State Sintering, *J. Am. Ceram. Soc.* 72 (1989) 810–817.
- [113] A. Pille, M. Amamra, A. Kanaev, F. Schoenstein, Microstructure and optical properties of alumina sintered from various phases, *Ceram. Int.* 45 (2019) 9625–9630.
- [114] P.C. Yu, F.S. Yen, On the High Pure Alumina Composite Powder for Sintering at 1400°C, A Preliminary Investigation, *Key Eng. Mater.* 313 (2006) 59–62.
- [115] P. Figiel, M. Rozmus, B. Smuk, Properties of alumina ceramics obtained by conventional and non-conventional methods for sintering ceramics, *J. Achiev. Mater. Manuf. Eng.* (2011).

- [116] G. Agarwal, R.F. Speyer, W.S. Hackenberger, Microstructural development of ZnO using a rate-controlled sintering dilatometer, *J. Mater. Res.* 11 (1996) 671–679.
- [117] I.-W. Chen, X.-H. Wang, Sintering dense nanocrystalline ceramics without final-stage grain growth, *Nature*. 404 (2000) 168–171.
- [118] R. Chaim, Liquid film capillary mechanism for densification of ceramic powders during flash sintering, *Materials (Basel)*. (2016).
- [119] V. Pouchly, K. Maca, Z. Shen, Two-stage master sintering curve applied to two-step sintering of oxide ceramics, *J. Eur. Ceram. Soc.* 33 (2013) 2275–2283.
- [120] M.P. Harmer, R.J. Brook, Fast firing-microstructural benefits, *J Br. Ceram Soc.* (1981).
- [121] D.J. Chen, M.J. Mayo, Rapid rate sintering of nanocrystalline ZrO₂-3 mol% Y₂O₃, *J. Am. Ceram. Soc.* (1996).
- [122] S.Y. Gómez, A.L. Da Silva, D. Gouvêa, R.H.R. Castro, D. Hotza, Nanocrystalline yttria-doped zirconia sintered by fast firing, *Mater. Lett.* (2016).
- [123] D.E. García, D. Hotza, R. Janssen, Building a sintering front through fast firing, *Int. J. Appl. Ceram. Technol.* (2011).
- [124] R. Kalousek, J. Spousta, J. Zlámál, P. Dub, T. Šikola, Z. Shen, D. Salamon, K. Maca, Rapid heating of zirconia nanoparticle-powder compacts by infrared radiation heat transfer, *J. Eur. Ceram. Soc.* (2017).
- [125] J. Zhang, F. Meng, R.I. Todd, Z. Fu, The nature of grain boundaries in alumina fabricated by fast sintering, *Scr. Mater.* (2010).
- [126] A. Kocjan, M. Logar, Z. Shen, The agglomeration, coalescence and sliding of nanoparticles, leading to the rapid sintering of zirconia nanoceramics, *Sci. Rep.* (2017).
- [127] W. Ji, B. Parker, S. Falco, J.Y. Zhang, Z.Y. Fu, R.I. Todd, Ultra-fast firing: Effect of heating rate on sintering of 3YSZ, with and without an electric field, *J. Eur. Ceram. Soc.* (2017).
- [128] C. Suryanarayana, Thermodynamics and Kinetics of Metastable Phase Transformation, in: *Non-Equilibrium Process. Mater.*, Elsevier, 1999: pp. 5–20.
- [129] S. Lamouri, M. Hamidouche, N. Bouaouadja, H. Belhouchet, V. Garnier, G. Fantozzi, J.F. Trelkat, Control of the γ -alumina to α -alumina phase transformation for an optimized alumina densification, *Boletín La Soc. Española Cerámica y Vidr.* 56 (2017) 47–54.

- [130] R.S. Mishra, C.E. Lesher, A.K. Mukherjee, High-Pressure Sintering of Nanocrystalline gammaAl₂O₃, *J. Am. Ceram. Soc.* 79 (1996) 2989–2992.
- [131] J. Croquesel, D. Bouvard, J.-M. Chaix, C.P. Carry, S. Saunier, S. Marinel, Direct microwave sintering of pure alumina in a single mode cavity: Grain size and phase transformation effects, *Acta Mater.* 116 (2016) 53–62.
- [132] S. Çınar, D.D. Anderson, M. Akinc, Influence of bound water layer on the viscosity of oxide nanopowder suspensions, *J. Eur. Ceram. Soc.* 35 (2015) 613–622.
- [133] A. Shafeiey, M.H. Enayati, A. Alhaji, The effect of slip casting and spark plasma sintering (SPS) temperature on the transparency of MgAl₂O₄ spinel, *Ceram. Int.* 44 (2018) 3536–3540.
- [134] M. Subbanna, P. Kapur, Pradip, Role of powder size, packing, solid loading and dispersion in colloidal processing of ceramics, *Ceram. Int.* 28 (2002) 401–405.
- [135] S. Çınar, D.D. Anderson, M. Akinc, Combined effect of fructose and NaCl on the viscosity of alumina nanopowder suspensions, *J. Eur. Ceram. Soc.* 35 (2015) 377–382.
- [136] Hamaker 2 - A software for Interparticle Interaction and Colloidal Stability Prediction, (n.d.).
- [137] M. Micháľková, K. Ghillányová, D. Galusek, The influence of solid loading in suspensions of a submicrometric alumina powder on green and sintered pressure filtrated samples, *Ceram. Int.* 36 (2010) 385–390.